First-principles study of intervalley mixing: Ultrathin GaAs/GaP superlattices

Robert G. Dandrea and Alex Zunger
Solar Energy Research Institute, Golden, Colorado 80401
(Received 17 October 1990)

First-principles pseudopotential calculations are reported for the structural properties, band offsets, and single-particle electronic states of $(GaP)_n(GaAs)_n$ (001) and (111) superlattices with $n \leq 3$. With the aim of developing a systematic theory to relate superlattice levels in these ultrathin systems to those of their constituents, the superlattice is treated as evolving from a virtual-crystal parent zinc-blende compound. A semiquantitative description of the resulting superlattice states evolves from this theory, which is based on (i) the small perturbative nature of the superlattice ordering potential with respect to this parent compound, (ii) a generic n dependence found for the intervalley coupling strengths, (iii) generic selection rules governing intervalley mixing, and (iv) observations of the dependence of coupling strengths on the anion versus cation character of the involved states. Application of these principles to (110) and (201) GaAs/GaP, and to the previously studied GaAs/AlAs systems, demonstrates their usefulness. Calculated energy gaps (and their direct versus indirect and type-I versus type-II character) are presented for the superlattices studied.

I. INTRODUCTION

Since Esaki and Tsu[1] first suggested the development of new semiconductor systems through the growth of two different materials in a layer-on-layer geometry, semiconductor heterostructures such as quantum wells and superlattices (SL's) have been one of the favorite modes of accomplishing band-gap engineering.[2-6] The basis for the band-gap variability provided by these layered structures is largely due to the fact that the resulting one-dimensional geometry causes a dipolar potential shift alternating (as a *constant*) in the quantum wells and barriers. For wide quantum-well structures (e.g., long-period SL's), where effective-mass theory is applicable, the resulting band-edge energy levels are then simply those of the constituents, modified by (i) the band-offset shift due to the dipolar potential, (ii) the confinement energy of the quantum well in which the state exists, and (iii) a strain splitting (if the constituents are lattice mismatched and the interfaces are coherent). The "engineering" of the levels then comes about controlling the amount of localization energy (by controlling the width of the well, or by controlling the growth direction that affects the pertinent effective mass) and by controlling the starting position of the constituent's band-edge energy levels (for example, by controlling alloy compositions of pseudobinary alloy constituents, or by controlling relative volume proportions or substrate lattice constants in coherent epitaxial growth of lattice-mismatched constituents). In the case of long-period strained-layer SL's, Osbourn[2] has demonstrated how such systems allow independent variability of structural properties (the lattice constant), optical properties (the band gap), and transport properties (carrier mobilities).

In contrast to this, levels in ultrathin SL's $[(AB)_n(A'B')_m$ with $n + m \leq 6]$ cannot be described by effective-mass theory. Other empirical theories (such as

tight-binding[7,8] or empirical-pseudopotential[9] theories) that incorporate the interface simply by averaging parameters from the bulk constituents describe such systems only approximately. In ultrathin SL's the interface region is a significant fraction of the total volume, and thus can cause strong mixings between different zinc-blende valleys that are folded on top of each other in the SL Brillouin zone. These mixings control the physics of energy levels in ultrathin SL's They cause energy-level splittings and repulsions (as large as 1 eV, as seen below) and oscillator strength sharing (thus controlling the pseudodirect versus direct nature of optical transitions). Such effects are largely peculiar to very-short-period SL's, and thus demonstrate the added flexibility these structures bring to the art of band-structure engineering. Such ultrathin SL's have been studied recently both experimentally and theoretically, especially with regard to the GaAs/AlAs (Refs. 10 and 11) and Si/Ge (Refs. 4 and 12) systems. A careful analysis of the physics controlling energy-level formation in such systems is particularly important, in light of the fact that spectroscopic analysis of the changes in their optical gaps is frequently used[13] as a probe in determining the extent of ordering in spontaneously ordered[14] ultrathin SL systems.

It is thus the purpose of this present work to apply self-consistent first-principles methods to systematically describe the physics of intervalley mixing and the resulting SL energy levels in short-period $(GaP)_n(GaAs)_n$ (001) and (111) SL's, with $n \leq 3$. Combining these results with corresponding results on the $(GaAs)_n(AlAs)_n$ system leads to the development of a general theory of energy-level formation in ultrathin SL's. This theory demonstrates, for example, that intervalley coupling strengths (and their resulting level repulsions and oscillator strength sharing) are very weak for even n period $(AC)_n(BC)_n$ SL's, and decay like $1/n$ for odd n periods. It gives a quantitative understanding to the degree to

which an optical transition in such systems is direct or pseudodirect, and to the degree to which it can be labeled type I or type II. We also present predictions for the optical transition energies in (001) and (111) $(GaP)_n(GaAs)_n$ SL's (Tables I and IV).

Previous work on intervalley mixings in SL's has been confined mainly to the (001) $GaAs/Al_xGa_{1-x}As$ common-anion system. In such a (001) SL geometry, the underlying zinc-blende X states are split into X^z (which folds to the SL zone center, and thus couples to the states at Γ there), and X^x and X^y (which couple to each other away from the SL zone center). Two basic questions have been attempted to be answered: (i) what is the strength of the Γ-X^z coupling at the SL zone center, and (ii) are the intervalley couplings experienced by X^{xy} and X^z, such as to cause the X^{xy} SL level to lie below the X^z level (possibly making the SL indirect in k space), in spite of the transverse X^{xy} mass being lighter than its longitudinal X^z counterpart. Regarding (i), understanding the Γ-X^z intervalley coupling is important since it directly affects measurable quantities such as optical efficiency, luminescence decay lifetime, and gap temperature dependence, which are used to assess the type-I versus type-II nature of SL energy gaps. The magnitude of this coupling has been extracted from the size of Γ-X^z anticrossings induced experimentally by varying applied electric[15] or magnetic[16] fields, and theoretically[8,9,17-23] by varying layer thicknesses, alloy composition, or external hydrostatic stress. With regard to topic (ii), recent experimental[10,24] studies have found that for $n=m \leq 3$, X^{xy} lies below X^z (in agreement with earlier calculations by Wei and Zunger[11]), whereas the effective-mass-determined order of X^z lying below X^{xy} holds for $n \geq 4$ In our discussion below on the common-cation GaP/GaAs system, we shall treat these same theoretical questions, and also generalize them to (111)-oriented SL's. As will be seen, comparison between the common-anion and common-cation systems will shed light on some of the underlying physics determining the answers to these questions.

There have been numerous experimental and theoretical studies of the (001) $GaP/GaAs_xP_{1-x}$ system. Indeed, these SL's were some of the very first ever to be grown.[25] By using a graded interlayer between the SL and a GaP substrate, Gourley et al.[26-29] have successfully grown strained-layer SL's without misfit dislocations through alternate metalorganic chemical-vapor deposition. Photoluminescence and absorption measurements were performed on samples with individual layer lengths between 60 and 250 Å (about 20–80 bilayers each), and As alloy composition x between 0 and 0.6. The first theoretical analysis of these strained-layer systems was given by Osbourn,[2,30] using both Kronig-Penney effective-mass theory and tight-binding calculations. Note that in such calculations the band offset is required as an input parameter. Osbourn, Biefield, and Gourley[29] originally found that their experimental data could be well characterized by such calculations that assumed a *vanishing* conduction-band offset of the unstrained constituents [i.e., that $\Gamma_{1c}(GaAs)$ lines up with $X_{1c}(GaP)$]. However, similar analysis of subsequent experimental data lead Gourley and Biefield[28] to arrive at a valence-band-offset

value of 0.60 eV (giving a conduction-band-offset value of 0.23 eV). In the short-period SL regime, Armelles et al.[31] and Recio et al.[32] have grown on GaAs substrates a set of $(GaP)_n(GaAs)_m$ SL's with $(n,m)=(2,6)$, (3,6), (4,6), and (5,7) by atomic-layer molecular-beam epitaxy. Type-I and type-II optical transitions were found from photoreflectance and photoluminescence measurements, respectively, while the E_1 and $E_1+\Delta_1$ transitions were obtained from ellipsometric measurements. Using the band offset as a fitting parameter, a multiband Kronig-Penney calculation was used to model the resulting measured SL transitions, from which a 0.4-eV conduction-band offset of the unstrained constituents was extracted. A subsidiary purpose of the present work is thus to resolve the disagreement between these experimental band-offset values through first-principles calculations.

The discussion will proceed as follows. The method used to perform the first-principles calculations will be described in Sec. II. Section III will outline the present theory of SL levels in ultrathin systems. Sections IV and V will demonstrate this theory for (001) and (111) SL's, respectively, with comparisons given between the common-cation GaAs/GaP and common-anion GaAs/AlAs systems. Section VI will explore briefly the nature of SL levels in [110] and [201] growth directions. A summary of our conclusions will be presented in Sec. VII.

II. METHOD OF CALCULATION

A self-consistent first-principles method is used in our calculations in order to be able to accurately describe the electronic charge rearrangement that occurs near the interface. This is crucial for a realistic description of the resulting intervalley mixing in the ultrathin SL systems considered here. In particular, we use density-functional theory[33,34] with a local-density approximation for the exchange-correlation potential.[35] A pseudopotential scheme is used to project out the core-electron degrees of freedom, with *ab initio* nonlocal semirelativistic pseudopotentials being generated by the method of Kerker.[36] With no corelike electronic wave functions to represent, a simple plane-wave basis set[37] can be used to represent the pseudovalence wave functions and corresponding density-functional potential. In the present calculations, wave functions are expanded in plane waves with kinetic energies up to 15 Ry, resulting in about 150 basis functions per atom. Brillouin-zone integrations are performed using Fourier quadrature, with SL k point sets chosen to be equivalent[38] to one of the special[39] k point sets of 2, 6, 10, or 28 points in the irreducible zinc-blende zone. Cell-external degrees of freedom are obtained through total-energy minimization, while cell-internal degrees of freedom are obtained by relaxing calculated Hellmann-Feynman forces.[37]

Apart from providing an accurate description of the interface, the first-principle methods used here also enable us to calculate reliable band offsets. This is important, as the band offset is one of the input parameters used in empirical theories that are needed for calculations

on longer-period SL's. The band offset is obtained by adding to the dipolar potential shift across the interface (which, in our calculations, is obtained[40] from the self-consistent SL charge density), the relevant band energies of the strained binary constituents.

The price to be paid for the use of these first-principles methods that provide accurate interfacial charge densities and valence-band energies is, as is well known,[41] an underestimation of band gaps by roughly 50%. This is due to the difference between the local-density-functional single-particle potential and the self-energy operator[34] that describes the true quasiparticles of the system. This problem is largely irrelevant for calculations of SL *valence*-band levels and *valence*-band offsets. In order to provide fairly accurate *conduction*-band information, however, we shall leave the realm of first principles and add to our calculated conduction-band states an energy shift that corrects for this band-gap problem. In order to present accurate conduction-band offsets, we will add the appropriate (different) shift for each conduction-band-edge level considered, thus circumventing the band-gap problem. Such a complete correction cannot be done for the SL conduction-band levels, however, since they are composed in general of states from both constituents and from different band edges within a single constituent. Although using a weighted-average gap correction[11] can partially correct for this, in this study we shall simply add a *single* constant gap correction to all SL conduction-band states. As our calculated gaps for GaP (at X_{1c}) and GaAs (at Γ_{1c}) underestimate experimental values by 0.82 and 0.92 eV, respectively, we have simply added a constant shift of 0.85 eV to obtain the conduction-band levels reported below.[42] The variation of this gap correction between the two constituents, and within the Brillouin zone of a given constituent, adds a total uncertainty of up to 0.15 eV to the energies of our resulting conduction-band levels. For example, the GaAs/AlAs SL levels we report below are all shifted by a constant gap correction of 0.92 eV from the originally calculated values. This allows their maximum difference with respect to the same levels calculated using a self-energy formalism[22] (that lacks the problem of band-gap underestimation) for the $n = 1$ and 2 (001) SL's to be less than 0.10 eV. The small uncertainty in conduction-band levels does not, however, greatly affect our major conclusions regarding the analysis of the origin of these states.

Empirical theories are critical for considering longer-period SL's (with more than 30 atoms per cell), which are beyond the scope of the first-principles methods used here. Such empirical theories, however, describe the interface by averaging parameters of the bulk constituents. Furthermore, the overlimitation of the basis set can lead to incorrect results. The problem[43] with nearest-neighbor tight binding (giving an infinite transverse X mass) is one prominent example, Also, both a one-band Wannier model[19] and an empirical-pseudopotential method that obtains the SL ordering potential from the difference of the constituent's form factors[44] have resulted in an incorrect description of the degeneracy and symmetry of the X^{xy} levels in (001) GaAs/AlAs SL's. These examples,

and the discussion above on the band-gap problem, demonstrate the strengths and weaknesses of both the first-principles and empirical methods. For the problem at hand, however, the first-principles method has been chosen in order to obtain an accurate description of intervalley mixings and splittings, in spite of the small uncertainty in conduction-band levels that it introduces.

III. GENERAL DESCRIPTION OF BAND-EDGE STATES IN ULTRATHIN SUPERLATTICES

In this section we present the general features of a theory that allows for semiquantitative understanding of the band-edge levels in ultrathin SL's. Its basic aim is to explain the physics of intervalley mixing, since this is largely what determines SL levels in ultrathin systems. We draw heavily on previous Wei and Zunger[11,45] in developing this theory. We shall consider the case of the band-edge levels of the (001) SL as an example. In the present section we shall *not* show any calculated SL levels, however. Rather, we demonstrate how the concepts developed here allow for an understanding of these states (i.e., their position with respect to the potential well formed by the constituent band edges, their degree of localization, and their degree of oscillator strength sharing), even without their actual calculation. In Secs. IV and V, the SL states resulting from actual first-principles calculations will be analyzed in terms of this general theory, in order to demonstrate its validity and usefulness.

A. Folding and coupling of the VCA states

Our present analysis of single-particle levels in ultrathin SL's is based on the observation that these levels are related closely to those of a virtual-crystal-approximation (VCA) parent binary Ga(AsP) compound. The physics underlying this is as follows: First, the pseudopotential of the virtual $\langle AsP \rangle$ anion is obtained from the appropriate weighted average of the As and P pseudopotentials. Second, the unit cell of $(GaP)_n(GaAs)_m$ SL can be decomposed into $n + m$ unit cells of the binary $Ga\langle AsP \rangle$ VCA compound, where the interface plane lattice constant is the same in the SL and VCA, and where the VCA constant in the SL growth direction is $1/(n + m)$ that of the SL (so that the VCA will be deformed from a a simple zinc-blende structure if the SL is not cubic). The VCA binary can be transformed into the SL by changing the virtual anion into As or P, and by allowing the appropriate distortions in each or the GaAs and GaP regions. We shall refer to this *gedanken* transformation of the VCA binary into the SL as "SL ordering" and the resulting difference $\delta V = V_{SL} - V_{VCA}$ between the self-consistent SL potential and that of its VCA parent as the "SL ordering potential." According to the above description of SL ordering, $\delta V(\mathbf{r})$ can be decomposed into a chemical and a strain component: $\delta V = \delta V_{chem} + \delta V_{str}$. Hence, δV_{chem} is the difference between the VCA self-consistent potential and that of an unstrained SL whose nuclear coordinates exactly match those of the underlying VCA binary structure (a "chemi-

cal" transformation of the virtual $\langle AsP \rangle$ anion into As or P being the only perturbation here), and δV_{str} is simply the remaining perturbation due to the distortions in each region of the SL (it is defined by $\delta V_{str} = \delta V - \delta V_{chem}$).

One immediate consequence of the commensurability of the SL and VCA unit cells is that, by Bloch's theorem, any SL state $|\Psi_{q\beta}\rangle$ with wave vector q in the SL Brillouin zone can be represented as a sum of VCA binary states $|\psi_{k\alpha}\rangle$ with exactly $n+m$ different k vectors in the large binary Brillouin zone. (α and β are band indices here.) Formally, this can be expressed as

$$|\Psi_{q\beta}\rangle = \sum_{k}^{n+m} \sum_{\alpha}^{\infty} A(k\alpha;q\beta)|\psi_{k\alpha}\rangle \ . \tag{1}$$

We say that these $(n+m)$ k vectors are *folded* onto the SL wave vector q, by the effect of the SL ordering potential. In the discussion below, we will, for simplicity, limit ourselves to the equal-period case $n=m$. In this case, if the shortest reciprocal-lattice vector of the VCA binary compound parallel to the SL growth direction is G; then the $2n$ VCA k vectors folded to the SL point q are

$$k_j = q + \frac{j}{2n} G \quad (j = -n+1, \ldots, n) \ . \tag{2}$$

Plotting the bands of the VCA binary compound along the line from $q - G/2$ to $q + G/2$ then shows all the VCA states that form the SL states at q.

As a concrete example we consider the band edges of (001) SL's, where $G/2 = X^z = (2\pi/a)(0,0,1)$. The 001 SL's with $n = m$ have space group D_{2d}^5 ($P\bar{4}m2$). As shown in Fig. 1., their Brillouin zone is simple tetragonal. We shall use a notation where k points in the SL zone are described with an overbar (e.g., $\bar{\Gamma}$). Consideration of the coordinates of the SL k points given in Fig. 1 implies [from Eq. (2)] that the $2n$ zinc-blende k points folded onto each SL point are as follows:

$$\bar{\Gamma} = \sum_{j=-n+1}^{n} \Gamma + \frac{j}{n} X^z = \Gamma + X^z + \cdots \ , \tag{3}$$
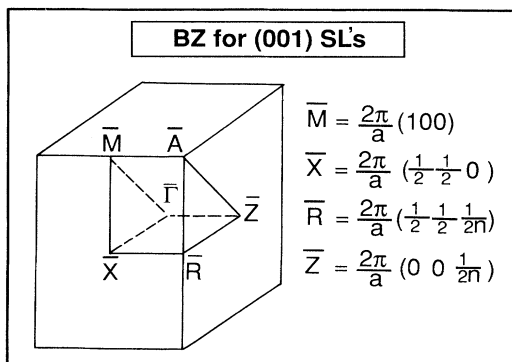
FIG. 1. Simple tetragonal Brillouin zone of (001) $(GaP)_n(GaAs)_n$ SL's.

$$\bar{M} = \sum_{j=-n+1}^{n} X^x + \frac{j}{n} X^z = X^x + X^y + \cdots \ , \tag{4}$$

$$\bar{L} = \sum_{j=-n+1}^{n} L_{111} + \frac{j}{n} X^z = L_{111} + L_{11\bar{1}} + \cdots \ . \tag{5}$$

Since L_{111} is folded to two different points in the SL zone depending on whether n is odd or even, we use the notation in Eq. (5) that $\bar{L} = \bar{R}$ for odd n, while $\bar{L} = \bar{X}$ for even n. Figure 2 shows the cubic VCA bands involved in the $a_{xy} = \bar{a}$ (001) SL band edges in their entirety. As an example, note that a zone-center state of an $(n,m) = (2,2)$ SL in the (001) orientation will be composed of states at four k points in the parent binary Brillouin zone at Γ, $\pm\frac{1}{2}X^z$, and X^z, which are all shown in Fig. 2(a). Similarly, the VCA states that fold to $\bar{M}$ in the SL zone are shown in Fig. 2(b), while those that evolve into $\bar{L}$ SL states are shown in Fig. 2(c). The three main zinc-blende band edges at Γ, X, and L are thus seen to fold to the three SL points $\bar{\Gamma}$, $\bar{M}$, and $\bar{L}$.

Note the manner in which strain splitting of the parent VCA levels affects the resulting SL states. For example, an equal-period SL will have a bulk equilibrium lattice constant very nearly at the average $\bar{a}$ of the two constituents. It will thus have a unit cell that is approximately cubic, and a VCA parent that is therefore just a zinc-blende structure. However, if one allows for the growth of only a very thin film (before the onset of misfit dislocations), such a SL can be grown away from $\bar{a}$ by coherent growth on a substrate with a different lattice parameter. The noncubic SL will have a VCA parent that is then deformed from its zinc-blende structure, resulting in a strain splitting of certain VCA band edges that are normally degenerate by cubic symmetry [e.g., X^{xy} splits from X^z in (001) SL's]. Figure 3 demonstrates the effect of such substrate lattice control on the VCA states of $Ga\langle AsP \rangle$ in both [001] and [111] growth directions. As we have described in detail elsewhere,[42] the main result of an increase in the substrate lattice parameter is a strong decrease in energy of the VCA $\bar{\Gamma}$ folding states (Γ_{1c} and X_{1c}^z for [001], Γ_{1c} and L_{1c} for [111]), while the non-$\bar{\Gamma}$ folding states remain comparatively higher in energy. This generic biaxial deformation-potential behavior implies that increasing the substrate lattice parameter strongly favors a transition to a more *direct*-gap SL.

A crucial result (to be demonstrated below), which allows for a straightforward relationship between the SL and VCA band edges, is that for the ultrathin SL's considered here, the SL ordering potential δV is sufficiently weak that within the infinite band sum of Eq. (1), only a very few (1–3) VCA states nearby in energy have significant expansion coefficients. We stress, however, that the smallness of this perturbation is only true in the ultrathin limit: due to the GaP-GaAs lattice mismatch of 4%, once a constituent's layer thickness becomes larger that just a few layers, the VCA to SL transformation would required changing a nuclear coordinate into a position of very dissimilar charge density (at $n = 25$, for example, cations are changed into anions, and vice versa). This would spread the spectral weight $A(k\alpha;q\beta)$ of SL wave functions over a much broader energy range of

(Figure 1 box content:)

BZ for (001) SL's

$\bar{M} = \frac{2\pi}{a}(100)$

$\bar{X} = \frac{2\pi}{a}(\frac{1}{2}\frac{1}{2}0)$

$\bar{R} = \frac{2\pi}{a}(\frac{1}{2}\frac{1}{2}\frac{1}{2n})$

$\bar{Z} = \frac{2\pi}{a}(0\ 0\ \frac{1}{2n})$
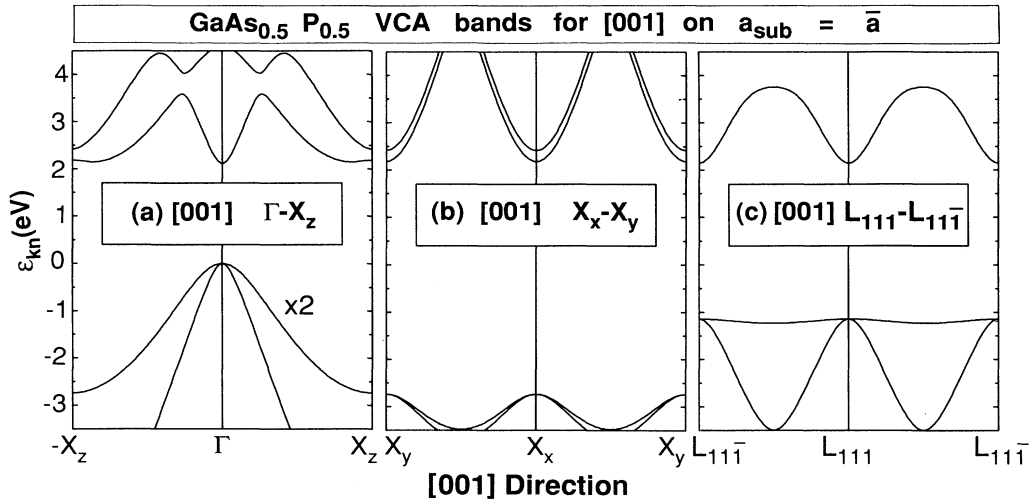
FIG. 2. Bands of the VCA Ga⟨AsP⟩ zinc-blende compound with lattice constant $\bar{a}$ along the (001) lines between the principal band-edge valleys. The bands in (a) are folded to $\bar{\Gamma}$, in (b) to $\bar{M}$, and in (c) to $\bar{L}$, in the SL zone.

VCA bands α.

The perturbative connection between ultrathin SL's and their parent VCA binary compound is the basis for the analysis of SL states to be presented below. This al-

lows for an immediate estimate of the strength of the intervalley mixing in the SL band edges simply by consideration of the energy separation of the involved VCA states shown in Fig. 2. Figure 2(a) shows that the SL
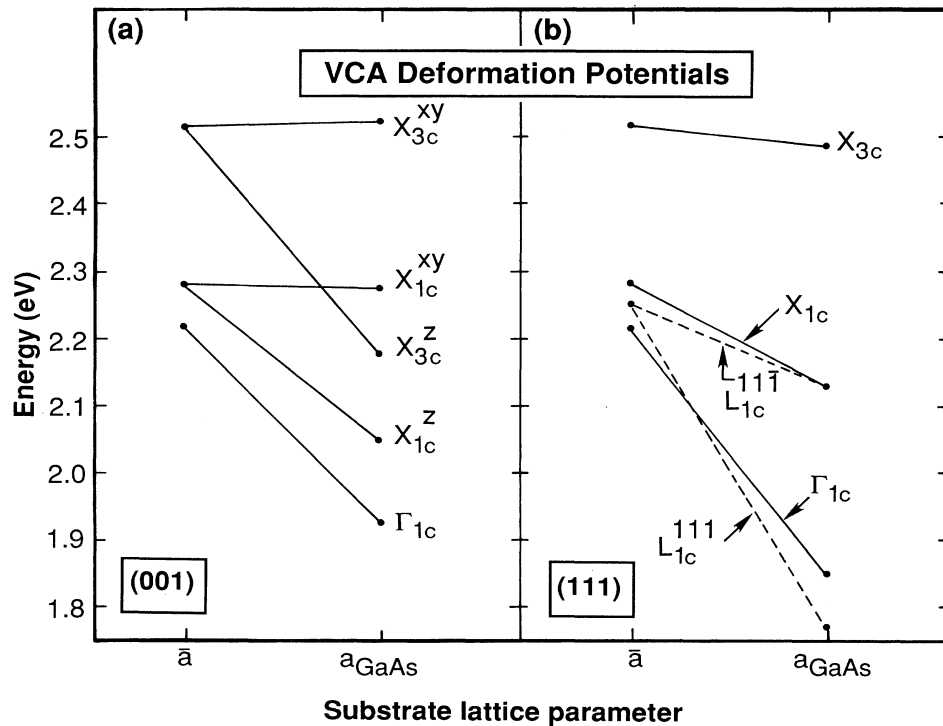
FIG. 3. Dependence of the VCA Ga⟨AsP⟩ conduction-band edges on substrate lattice constant.

valence-band-maxima states at $\bar{\Gamma}$ will evolve from within a single VCA valley (since the nearest X^z states is over 2 eV away), but that both conduction- and valence-band edges at $\bar{M}$ and $\bar{L}$ will evolve from states from two degenerate VCA valleys (and will thus have potentially large first-order splittings). Similarly, the conduction-band-edge states at $\bar{\Gamma}$ will also show strong intervalley mixing (and oscillator strength sharing) because of the closeness in energy of the VCA Γ and X^z conduction-band valleys.

Consider, furthermore, the degree of involvement in the SL band edge of VCA states at intervening **k** points also included in the folding when $n \geq 2$ [i.e., the points $\frac{1}{2}$ (for $n = 2$) or $\frac{1}{3}$ and $\frac{2}{3}$ (for $n = 3$) the way between the main valleys]. When the (001) band dispersion is quite flat [as it is for the valence-band maxima between L_{111} and $L_{11\bar{1}}$; see Fig. 2(c)], reflecting a heavy-mass VCA band edge, these intervening states will be strongly mixed into the resulting SL level. However, when the VCA band edge is of light mass [e.g., the conduction-band edge at X^{xy} in Fig. 2(b)], these intermediate **k** points will give rise to too-large energy denominators to be involved in the SL band-edge state. The implication of this to the degree of localization of the resulting SL state is straightforward: localization in a given region of the SL requires mixing of VCA states, which are at the *minimal* nearby distance $\delta k = G/2n$ in **k** space. This follows from standard concepts[46] of Fourier analysis: if a SL wave function Ψ is composed of several VCA wave functions ψ_i, so that

$$\Psi(\mathbf{r}) = \sum_i u_i(\mathbf{r}) e^{i\mathbf{k}_i \cdot \mathbf{r}} , \qquad (6)$$

where $u_i(\mathbf{r})$ is periodic in a VCA binary unit cell, then the *maximum* period of its squared norm

$$|\Psi(\mathbf{r})|^2 = \sum_{i,j} u_i(\mathbf{r}) u_j^*(\mathbf{r}) e^{i(\mathbf{k}_i - \mathbf{k}_j) \cdot \mathbf{r}} \qquad (7)$$

is 2π times the reciprocal of the *minimum* value of $\delta k = \mathbf{k}_i - \mathbf{k}_j$. In the present case of equal-period (001) SL's with total period of length na, SL wave functions are made [see Eqs. (3)–(5)] of VCA states separated by $\delta k = X^z/n = 2\pi/na$, and thus require these *neighboring* **k** states to localize in one-half of the SL. For example, a $\bar{\Gamma}$ state in an $n = 3$ (001) SL cannot be localized by mixing Γ and X^z, but must result from mixing Γ and $\pm\frac{1}{3}X^z$, or X^z and $\pm\frac{2}{3}X^z$. This, of course, is the origin of the standard result from effective-mass theory: heavy-mass states localize readily in their quantum wells, while light-mass states remain more delocalized.

It is worth mentioning the complementarity of the present VCA-based representation of SL states, and the frequently used "slab" representation, where an $(AB)_n(A'B')_m$ SL state is described in terms of both propagating and evanescent AB binary states in the AB part of the SL, and of similar $A'B'$ states in its region of the SL. This slab representation is the basis for envelope-function-based effective-mass theories,[47] and of other empirical theories that use a small localized basis set (such as tight binding[48] or Wannier orbitals[19]). In our current discussion, however, we shall describe SL states

$|\Psi_{q\beta}\rangle$ in terms of VCA states $|\psi_{\mathbf{k}\alpha}\rangle$ that extend throughout the whole SL. This representation of SL states is complementary to the slab representation: for the ultrathin SL's considered here (with layer widths *not* longer than evanescent state decay lengths), the VCA representation is preferable, while for longer-period SL's, the slab representation more directly provides the connection between the states of the SL and those of its constituents.

Finally, we stress the VCA states (which we currently treat as the SL parent states because they minimize the SL ordering perturbation) are approximately at the average energies of the two zinc-blende constituents.[49] These average energies can thus simply be used in future practical applications of this current theory.

B. Single-valley states

Our foregoing discussion shows that SL states that evolve from *within* a single VCA band-edge valley (like the valence-band-maxima states at $\bar{\Gamma}$) will qualitatively obey the long-period Kronig-Penney effective-mass theory. The *intra*valley mixing of VCA states separated by minimal $\delta k = G/2n$ results in an envelope-function nature to their wave function, which allows the band-edge levels of the strained constituents to act as an actual potential well. With increasing period n, their energy levels will thus fall from their parent VCA energy (which is approximately at the center of the potential well[49]) to the energy of the well bottom. Concomitantly, their wave functions will become increasingly localized on that SL partner whose band edge acts as the potential well, and not the barrier. Note that knowledge of the actual band offsets is needed to describe these single-valley SL levels, because they have begun to Kronig-Penney-localize.

C. Multiple-valley states

In contrast to these single-valley states, most of the other band-edge levels in these ultrathin SL's will experience substantial *inter*valley mixing. As seen in Fig. 2, this will occur in the conduction-band levels at $\bar{\Gamma}$ [Fig. 2(a)], and in both conduction- and valence-band edges at $\bar{M}$ and $\bar{L}$ [Figs. 2(b) and 2(c)]. The strength of this coupling between two VCA states $\psi_1(\mathbf{k})$ and $\psi_2(\mathbf{k}+G/2)$ from valleys separated by $G/2$ is determined by the magnitude of the matrix element $U = \langle \psi_1(\mathbf{k})|\delta V|\psi_2(\mathbf{k}+G/2)\rangle$.

Consider first the behavior of SL states made from two band-edge VCA states separated by $G/2$, *without* much involvement of the VCA states from the intervening **k** points. This behavior will occur frequently in ultrathin SL's because of the fairly large energy differences between VCA band edges and states $\delta k = G/2n$ away when $n \leq 3$ or 4. (These energy differences will of course vanish as n increases and δk decreases, and the states from the intermediate **k** points will become involved in the then Kronig-Penney-type SL state.) The SL states are thus determined by the 2×2 Hamiltonian matrix whose off-diagonal term is U. If the diagonal elements are just the VCA energies ε_1^0 and ε_2^0 (Appendix A explains the near vanishing of the diagonal elements of δV), the resulting

SL energies are just

$$\varepsilon_\pm = \frac{\varepsilon_1^0 + \varepsilon_2^0}{2} \pm \left[\left[\frac{\varepsilon_1^0 - \varepsilon_2^0}{2} \right]^2 + |U|^2 \right]^{1/2} . \qquad (8)$$

In the case of mixing two nondegenerate VCA levels, U determines the magnitude of the level repulsion, while the ratio $2U/(\varepsilon_2^0 - \varepsilon_1^0)$ determines the amount of wavefunction mixing. In the case of the mixing of two degenerate VCA states (i.e., $\varepsilon_1^0 = \varepsilon_2^0$), the magnitude of the resulting first-order level splitting is just $\Delta\varepsilon = 2|U|$, while the SL wave function is always just the equally weighted even or odd combinations of the two VCA states ψ_1 and ψ_2, regardless of the size of U.

A major result (derived in Appendix A) is that there is a universal n dependence to this intervalley coupling strength U: it is comparatively small for even n, while for odd n it is found to decay from its maximal $n=1$ value like $1/n$. This behavior results from the manner in which the $e^{i\mathbf{G}\cdot\mathbf{r}/2}$ phase factor (due to the product of two VCA wave functions separated by $\mathbf{G}/2$) couples to the SL ordering potential δV, which is approximately odd with respect to inversion about an interface. This generic n dependence is seen both when symmetry forces intervalley mixing between two degenerate VCA states [e.g., between X^x and X^y in Fig. 2(b) or between L_{111} and $L_{11\bar{1}}$ in Fig. 2(c)] and in cases of intervalley mixing between nondegenerate VCA states [e.g., between Γ and X^z in Fig. 2(a)]. In the former case the level splittings will oscillate with n, nearly vanishing for even n, while decaying like $1/n$ for odd n. This result is symmetry imposed, and has previously been noted by Froyen et al.[50] In the case of the interaction between nondegenerate VCA states, this results in a level repulsion that oscillates similarly with n, and in a commensurate oscillation in the degree of oscillator strength sharing.

The effects on the symmetry-imposed mixing between two degenerate VCA states are particularly striking. In this case, since the SL states are made of equally weighted portions of VCA binary states separated by $\delta k = \mathbf{G}/2$, their wave functions segregate into every second VCA unit cell [see Eq. (7)], and Wei and Zunger[11] have thus labeled such SL states segregating levels. We distinguish here the behavior of even versus odd n. For even n, the SL states will be completely delocalized, and the two degenerate VCA levels will remain unsplit because the even and odd combinations $\psi_1 \pm \psi_2$ are equally delocalized (both having half their norm in each half of the SL). The unsplit levels will lie just at the middle of the potential well formed by the band-edge levels of the strained constituents, because this midpoint is just the energy of the parent VCA levels.[49] For odd n, their partial degree of localization will decay like $1/n$, with some remnant of localization existing due to the partial commensurability of their every-second VCA cell segregation pattern with a SL half-period when n is odd. (This localization behavior will be demonstrated pictorially in Sec. IV.) Since the disparity in the degree of partial localization between the even and odd combinations also decays like $1/n$, the SL level splitting also behaves proportionately.

For $n \geq 2$ (even or odd), such states are resonant

throughout the SL, because they are not composed of VCA states separated by minimal $\delta k = \mathbf{G}/2n$, and thus cannot localize in one-half of the SL unit cell. Nonlocalizing SL states such as these are frequently referred to as resonant levels, and the analysis above explains why such resonant levels generally lie near the midpoint of the potential well made by the constituent's band edges: at that energy they are resonant with their VCA zinc-blende parent states, leading to a spectral decomposition that reflects this, and a resulting periodicity that is more zinc-blende-like than that required to localize in one-half of the SL unit cell.

This characteristic n dependence is also approximately seen in the intervalley mixing of nondegenerate VCA states that are not forced to mix by symmetry. In the case of the mixing of the VCA conduction-band-edge levels at Γ and X^z, it means that the level repulsion will be comparatively small for even n period SL's and will decay like $1/n$ for odd n periods, and that the amount of oscillator strength sharing will be similar. This explains the observation[8,9,15–22] of a decrease with n in the $\Gamma_{1c}\text{-}X_{1c}^z$ coupling strength found in (001) GaAs/Al$_{1-x}$Ga$_x$As.

D. Selection rules

Understanding the coupling between VCA states requires knowledge of the selection rules governing the matrix elements $\langle \psi_1(\mathbf{k}) | \delta V | \psi_2(\mathbf{k}+\mathbf{G}/2) \rangle$. These are derived in Appendix B. As an example, we simply mention two of the more important ones appropriate to (001) SL's. With regard to the intervalley mixing at $\bar{\Gamma}$ between the VCA Γ and X^z conduction-band-edge states, Appendix B shows that in common-cation (-anion) systems, it is only the lower (upper) X^z conduction-band minimum[51] that mixes for odd n, while the reverse mixing is only allowed for even n. With regard to the mixing of the degenerate VCA X^x and X^y conduction-band-edge states at $\bar{M}$, Appendix B shows that in common-cation (-anion) systems only the lower (upper) X^{xy} levels split for odd n, while for even n exactly the reverse is true.

E. Magnitude of intervalley coupling strengths

The magnitude of the splittings and level repulsions resulting from intervalley mixing of symmetry-compatible states reflects the properties of the perturbation δV. In a lattice-matched common-anion system such as GaAs/AlAs, $\delta V_{\text{str}} = 0$, and δV_{chem} is largely an s-like function[52] centered on the mixed cation sublattice. Hence states with a large amount of cation-s character will couple strongly to this δV. We thus expect large repulsions and mixings between the VCA Γ_{1c} and upper X^z conduction-band minimum at $\bar{\Gamma}$, and large first-order splittings of the upper X^{xy} conduction-band minima at $\bar{M}$ and of the VCA L_{1c} states at $\bar{L}$. In a common-cation system such as (001) GaAs/GaP, however, δV has both a chemical piece δV_{chem} that is anion-s centered and a strain piece δV_{str} that has p_z character on both sublattices. The level splittings and repulsions mentioned above (now involving the lower X conduction-band states, however) are thus expected to be smaller than in

GaAs/AlAs. As will be shown in Sec. IV, this is indeed found in our calculations, with 1-eV splittings at $\overline{M}$ and $\overline{L}$ in GaAs/AlAs, but only 0.1–0.5-eV splittings in GaAs/GaP (with a similar comparison holding for the Γ-X^z coupling strength at $\overline{\Gamma}$).

F. Summary of the model

In summary, our present theory of the band-edge levels in ultrathin SL's is as follows: Noting that the SL ordering potential δV only mixes VCA parent states that are nearby in energy (less than about 0.5–1 eV), the nature of the SL band-edge states at wave-vector $\mathbf{q}$ can be predicted simply by observation of the dispersion of the VCA bands along the line $\mathbf{q}-\mathbf{G}/2$ to $\mathbf{q}+\mathbf{G}/2$. There are two generic cases. (i) When only one VCA valley is involved in the band edge at $\mathbf{q}$, the resulting SL states will qualitatively obey the Kronig-Penney effective-mass theory: as n increases, the SL levels will fall from the average energy of the strained constituent band edges (which is just the parent VCA energy at the well center) down into the well bottom, with a commensurate localization of the SL wave function. For the small n values considered here, however, the qualitative amount of confinement energy will of course not simply be the particle-in-a-box value $\hbar^2\pi^2/2m^*L^2$, because the length scale is not large enough to allow for a complete envelope-function localization of the SL wave function. Rather, from the examples considered below, we will see that by $n=3$ the SL level will generally fall from the middle height in the well (50%) to the 25–40 % level (depending on how heavy the VCA mass is). (ii) The other generic type of state seen in these ultrathin SL's arises from mixing between VCA valleys separated by $\mathbf{G}/2$. This intervalley mixing is quite strong in these short-period SL's because of the proportionately large effect of the interface, and thus gives rise to level splittings and repulsions as large as 1 eV, and similarly large oscillator strength sharing. As will be demonstrated in Secs. IV–VI, such physical manifestations of this mixing can be predicted semiquantitatively with the aid of the knowledge of the generic n dependences, selection rules, and common-anion versus common-cation differences that were explained above.

IV. RESULTS FOR (001) SUPERLATTICES

In this section we present the results for the structural properties, band offsets, and SL electronic levels for (001) $(GaP)_n(GaAs)_n$ SL's, with $n=1$, 2, and 3. The results will be analyzed in terms of the model advanced in Sec. III.

A. Structural properties

Equilibrium lattice constants of the constituent zinc-blende compounds are obtained by standard total-energy minimization. For GaP, a value of 5.406 Å is calculated (0.8% error), compared to an experimental value[53] of 5.4505 Å. For GaAs, we calculate 5.614 Å (0.7% error), while experiment[53] gives 5.6537 Å.

Throughout this study, we use the *calculated* equilibria of the zinc-blende constituents in order to obtain the lattice constant of the SL's and of the strained binary constituents. We assume that the in-plane SL lattice constant a_{xy} is simply its equilibrium value, which is (since we consider only $n=m$ equal-period SL's) just the average $\overline{a}=5.510$ Å of the calculated equilibrium lattice spacings of the two constituents.[54] (See, however, Fig. 3 for the results of coherent SL growth on a substrate with lattice parameter different from the equilibrium SL lattice constant $\overline{a}$.) The spacings of the atomic planes in the z direction are obtained as follows. First, the equilibrium atomic configurations of the "epitaxially constrained" binary constituents are calculated, by minimizing the total energy of the binary compounds with respect to (001) tetragonal distortions, keeping the in-plane lattice constant $a_{xy}=\overline{a}$ fixed. This results in calculated tetragonal distortions of $c/\overline{a}=0.966$ for GaP and $c/\overline{a}=1.034$ for GaAs, in good agreement with harmonic elasticity theory.[54] Note that the smaller GaP, being *extended* in the xy plane, reacts by a tetragonal *compression* in the z direction, and vice versa for GaAs. The (001) SL's are then constructed simply by layering together slabs of these epitaxially constrained binary constituents. Since the average of the tetragonal distortions of the binaries is unity, the resulting $n=m$ SL's will always be cubic (and the parent VCA compound will simply be a zinc-blende structure with lattice constant $\overline{a}$). The layer spacings constructed by the above method were then tested by calculations of the resulting Hellmann-Feynman forces on the atoms in the SL. These forces were always found to be negligible, demonstrating the validity of the above construction.

As we have pointed out in a previous publication,[54] no further interfacial relaxations are found here due to the symmetry of interfacial atoms in this (001) geometry with a common atom (in our case, Ga). In that same study,[54] we also reported the small positive formation energies of these (001) and (111) GaP/GaAs SL's; no further reference to the stability of these SL's will be given here.

B. Band offsets

The band offset is extracted from a straightforward analysis[40] of the self-consistent charge density of the $n=3$ (001) SL. We find that the charge density in that part of the SL that is not within about 1 Å of an interface is exactly the same as that of the isolated (but strained) constituent binary compound (there being a small amount of charge relaxation constrained to the interface region). This means, because of the one-dimensional geometry of the SL, that the potential in this noninterface region is the same as that of the strained constituent, apart from a constant which represents the alternating dipolar potential shift. Analysis of the classical Coulomb potential resulting from the charge density of the $n=3$ SL then allows this dipolar potential shift to be evaluated,[40] whence the bands of the strained binary constituents can then be put on a common energy scale. The resulting band lineups are shown in Fig. 4, where the spin-orbit splittings have been included in the valence-band edges.

Neglecting spin-orbit effects results in a triply degenerate Γ_{15v} zinc-blende valence-band maximum being split by the crystal field into a Γ_{5v} doublet and a Γ_{3v} singlet in the strained binary compounds. The crystal-field (CF) splitting is

$$\Delta_{CF} = \varepsilon(\Gamma_{5v}) - \varepsilon(\Gamma_{3v}) \qquad (9)$$

and the average energy is

$$\varepsilon_{av} = \tfrac{2}{3}\varepsilon(\Gamma_{5v}) + \tfrac{1}{3}\varepsilon(\Gamma_{3v}) \ . \qquad (10)$$

Aligning these strained binary states on an absolute energy scale as explained above, we find the following energies (all in eV): for GaAs, $\Gamma_{5v} = 0$ and $\Gamma_{3v} = -0.20$, while for GaP, $\Gamma_{5v} = -0.52$ and $\Gamma_{3v} = -0.34$ [see also Fig. 2(b) of Ref. 42]. Including spin-orbit effects, the zinc-blende valence-band maxima are composed of a Γ_{8v} doublet (light-hole plus heavy-hole states) and a Γ_{7v} spin-orbit split-off state. The Γ_{8v}-Γ_{7v} energy separation is defined as $\Delta_{s.o.}$ (where s.o. denotes spin orbit). The strain caused by lattice mismatch then splits the Γ_{8v} light- and heavy-hole doublet and mixes the light-hole state with the Γ_{7v} spin-split state. To quantitatively describe the interplay of noncubic crystal fields and spin-orbit splittings, we use

the quasicubic model of Hopfield.[55] In this approximation, the heavy-hole state is

$$\varepsilon(\Gamma_{6v}) = \varepsilon_{av} + \tfrac{1}{3}(\Delta_{s.o.} + \Delta_{CF}) \ , \qquad (11)$$

while the light-hole and spin-split states mix to form two states at

$$\varepsilon(\Gamma_{7v}^{\pm}) = \varepsilon_{av} - \tfrac{1}{6}(\Delta_{s.o.} + \Delta_{CF})$$
$$\pm \tfrac{1}{2}[(\Delta_{s.o.} + \Delta_{CF})^2 - \tfrac{8}{3}\Delta_{s.o.}\Delta_{CF}]^{1/2} \ . \qquad (12)$$

Comparison of these model energies with fully relativistic all-electron calculations[56] show them to err by less than 5 meV. We thus use these model energies to incorporate spin-orbit effects into our calculated valence-band offsets. We use spin-orbit splittings $\Delta_{s.o.} = 0.34$ eV for GaAs and $\Delta_{s.o.} = 0.08$ eV for GaP.[57]

The resulting band-offset diagram of Fig. 4 shows that the overall valence-band offset is 0.44 eV between the GaAs heavy-hole state and the upper GaP light-hole plus spin-split state. The overall conduction-band offset is 0.09 eV between the GaAs Γ and GaP X^z conduction-band minima. We stress that these calculated offsets are for the bands of the *strained* constituents, because the $n=3$ SL from which they were extracted is a strained-layer SL with coherent interfaces. Both constituents thus have $a_{xy} = \bar{a}$, while the GaP has undergone a tetragonal compression with $c/a = 0.966$, and the GaAs has $c/a = 1.034$.

There have been four experimental attempts to determine the GaP/GaAs band offsets. Two of these have been on thin strained-layer SL's, while the other two have used systems with incoherent interfaces (any strain being relieved by misfit dislocations), resulting in unstrained constituents. The first attempt, by Davis et al.,[58] was done by analyzing current-voltage transport data of an interface obtained by growing a thick film of GaAs on GaP (resulting in unstrained constituents). They found a vanishing conduction-band offset $\Delta E_c = 0$ (giving a valence-band offset $\Delta E_v = 0.83$ eV). Such an offset is consistent with electron affinity data.[29,30] An indirect measurement of the unstrained offset was done by Katnani and Margaritondo,[59] who performed photoemission measurements of GaAs and GaP on Si and Ge, and then used a transitivity assumption to extract a GaP/GaAs valence-band offset of $\Delta E_v = 0.55$ eV (GaAs higher) for the unstrained constituents (which gives $\Delta E_c = 0.28$ eV).

With regard to measurement of the offset at the coherent strained-layer interface, Gourley, Biefeld, and Osbourn[28,29] have performed photoluminescence and excitation (absorption) experiments on (001) $(GaP)_n(GaAs_xP_{1-x})_n$ SL's with n in the range 20–80 and $x \leq 0.5$. Because the lattice mismatch of GaP with these $x \leq 0.5$ alloys is less than half that with pure GaAs, the layer widths here are sufficiently short to allow this mismatch to be accommodated by a small strain. Originally,[29] the vanishing conduction-band-offset value from electron affinity and transport measurements[58] was assumed in the theoretical analysis of their measurements. More recently, however, Gourley and Biefeld[28] have modeled their measured SL energy levels using Kronig-
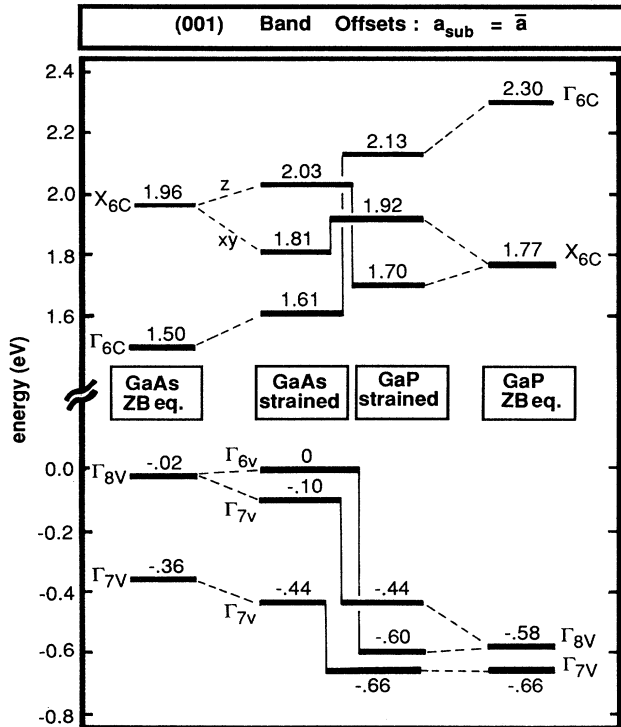
FIG. 4. Calculated band offsets of the (001) GaAs/GaP coherent interface, for the strain conditions appropriate to equal-period SL's (i.e., $a_{xy} = \bar{a}$). The offsets of the unstrained constituents are obtained from these strained binary offsets through the absolute deformation-potential model of Ref. 60, which is used only to line up the valence-band maxima at Γ.

Penney theory, using the valence-band offset as a fitting parameter. However, rather than report the offsets of the strained constituent bands, they used an absolute deformation-potential model[60] to relate these levels to those of their zinc-blende equilibria parent compounds. Furthermore, they interpolated the offset to $x=1$ alloy composition (i.e., GaP/GaAs). They thus reported a valence-band offset $\Delta E_v = 0.60 \pm 0.05$ eV (with GaAs being higher) for the *unstrained* binary constituents. (This gives a conduction-band offset $\Delta E_c = 0.23$ eV.) Recio et al.[32] have performed a very similar analysis on their spectroscopic measurements of short-period $(GaP)_n(GaAs)_m$ SL's with n between 2 and 5 and m equal to 6 or 7. Rather than present offset data for the strained constituents, they similarly report offsets only with respect to the *unstrained* constituents. They find a conduction-band offset $\Delta E_c = 0.40$ eV, with the GaAs Γ state being lower than the GaP X conduction-band minimum. (This gives $\Delta E_v = 0.43$ eV.)

Note that all four experimental analyses have reported offsets only with respect to the *unstrained* constituents, regardless of the particular strain state of the GaP and GaAs in the actual sample that was used. There seems to be two reasons that some type of absolute deformation-potential analysis is frequently used to "back out" of the actual strained-layer offsets those of the unstrained constituents. First, there is a simple "bookkeeping" reason: the variability in the n/m ratio allows for a multitude of different strain states of the constituents, and further variability results from the alloy composition x. All these n/m and x-dependent offsets should, however, be consistently related to the *same* unstrained $x=1$ offset by a common model, and it is thus easier to tabulate this latter offset value. Second, there seems to be a belief that the resulting *unstrained* offset value that is extracted from a thin strained-layer SL is identical to the value obtained from a thick-layered unstrained sample with an incoherent interface. Whatever the reasons, this practice of reporting only offsets for the unstrained constituents is, as seen in the present example, quite prevalent. In order for us to compare our calculated offsets with experiment, we are also forced to extract from them their unstrained values. We do this using the same absolute deformation-potential model[60] as used by Gourley and Biefeld. In this model, the absolute shift in the average energy of the three valence-band-maxima states in going from the equilibrium zinc-blende to the strained binary structure is due only to the isotropic component of the strain, it being assumed that the shear component only shifts these three levels relative to each other. In the present case the isotropic strain component is -0.0074 for GaAs and $+0.0077$ for GaP. Within this model,[60] the GaAs compression results in the Γ_{8v} and Γ_{7v} valence-band states decreasing 0.042 eV in energy (in an absolute sense), while the GaP tension causes these states to raise 0.043 eV. These shifts are used to present the offsets of the unstrained constituents shown in Fig. 4 The resulting valence-band offset of 0.56 eV is in excellent agreement with the experimental results of Gourley and Biefeld[28] (0.60 eV) and of Katnani and Margaritondo[59] (0.55 eV), but the conduction-band offset of 0.27 eV is in small

disagreement with the 0.40-eV value of Recio et al.,[32] and in strong disagreement with the 0.0-eV value from the early transport[58] and electron affinity measurements. We stress, however, that our calculations really only permit an accurate description of the offsets of the strained constituents. The absolute deformation-potential model used here[60] is quite crude, there being much recent work in improving these models.[61] It was used only to permit a consistent comparison to the experimental work of Gourley and Biefeld, who used the same model. A more accurate analysis of the unstrained offsets for an incoherent interface would require the inclusion of the effects of misfit dislocations on the dipolar potential shift. Such a calculation is beyond our present scope.

There has been, to the authors' knowledge, only one other theoretical calculation of the GaP/GaAs band offset. Tersoff[62] has used a model whereby the midgap neutrality levels of the unstrained constituent zinc blendes are aligned to predict a valence-band offset of 0.31 eV (GaAs higher). This is 0.25 eV smaller than that calculated here.

C. Superlattice energy levels

We now present the analysis of the calculated single-particle electronic energy levels of the (001) SL's in terms of the model of Sec. III. Table I gives our calculated energy gaps for the $n=1$, 2, and 3 SL's.

The analysis of energy levels of ultrathin SL's presented in Sec. III was based on the perturbative connection between such levels and those of their VCA parent compound. The smallness of the perturbation caused by the SL ordering potential δV can be clearly seen in Fig. 5, where the Γ-X bands of the VCA zinc-blende structure
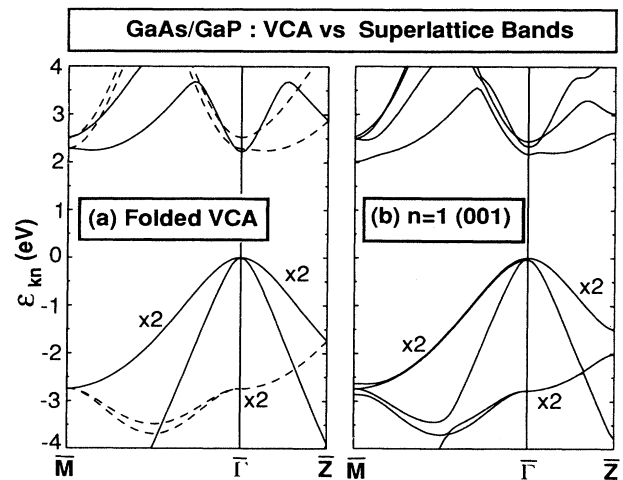
FIG. 5. Band structure of (a) the VCA Ga$\langle$AsP$\rangle$ zinc-blende parent compound, and (b) the (001) $(GaAs)_1(GaP)_1$ SL for substrate lattice constant $a_{sub} = \bar{a}$. In (a), the bands folded into the SL zone are shown as dashed lines. Doubly degenerate bands are marked "$\times 2$."

TABLE I. Principal conduction-band edges of the $(GaP)_n(GaAs)_n$ (001) SL's in relation to their parent VCA levels. In the cases of $\overline{M}$ and $\overline{L}$, $\Delta\varepsilon$ is the splitting of the two degenerate VCA levels that fold there. All energies are in eV, and are measured with respect to the respective valence-band-maximum state at Γ or $\overline{\Gamma}$, neglecting spin-orbit effects. (These can be included by subtracting 0.07 eV from all energies here.) The asterisk in each column denotes the conduction-band minimum. A gap correction of 0.85 eV was added to all calculated conduction-band energies here. [Note that in our previous study of the $n=1$ SL (Ref. 42), a shift of only 0.75 eV was applied to the same values. The results in this table are thus 0.1 eV larger than those in Ref. 42.]

Origin	VCA Anion	$n=1$ Anion	$n=2$ Cation	$n=3$ Anion
Γ	$\Gamma_{1c}=2.22^*$	$\overline{\Gamma}_{1c}=2.17$	$\overline{\Gamma}_{1c}=2.21^*$	$\overline{\Gamma}_{3c}=2.15^*$
	$X_{1c}^z=2.28$	$\overline{\Gamma}_{1c}=2.34$	$\overline{\Gamma}_{3c}=2.24$	$\overline{\Gamma}_{1c}=2.15$
	$X_{3c}^z=2.52$	$\overline{\Gamma}_{3c}=2.44$	$\overline{\Gamma}_{1c}=2.32$	$\overline{\Gamma}_{1c}=2.19$
$\overline{M}$	$X_{1c}^{xy}=2.28$	$\overline{M}_{2c}=2.01^*$	$2\overline{M}_{5c}=2.26$	$\overline{M}_{1c}=2.16$
		$\overline{M}_{1c}=2.54$		$\overline{M}_{2c}=2.33$
	$X_{3c}^{xy}=2.52$	$2\overline{M}_{5c}=2.50$	$\overline{M}_{1c}=2.486$	$2\overline{M}_{5c}=2.47$
			$\overline{M}_{2c}=2.487$	
$\Delta\varepsilon$		0.522	0.001	0.173
$\overline{L}$	$L_{1c}^{111}=2.25$	$\overline{R}_{3c}=2.19$	$\overline{X}_{1c}=2.223$	$\overline{R}_{1c}=2.19$
	$L_{1c}^{1\overline{1}\overline{1}}=2.25$	$\overline{R}_{1c}=2.28$	$X_{3c}=2.225$	$\overline{R}_{3c}=2.22$
$\Delta\varepsilon$		0.089	0.002	0.030

are compared to the corresponding $\overline{\Gamma}\text{-}\overline{M}$ and $\overline{\Gamma}\text{-}\overline{Z}$ bands of the $n=1$ (001) SL. (The VCA zinc-blende bands have been folded into the SL Brillouin zone for ease of comparison.) Except for the large (0.5-eV) first-order splittings at $\overline{M}$ and $\overline{Z}$ ($\pm\frac{1}{2}X^z$ are folded onto $\overline{Z}$), and the rather smaller energy shifts due to second-order level repulsions elsewhere in the zone, the two sets of bands are extremely similar. The maximum 0.5-eV shifts between the VCA and SL bands in Fig. 5 reflect the fact that only VCA states within about 0.5 eV are mixed by the SL ordering potential. It is this basic fact that allows the straightforward connection between VCA and SL levels.

Figure 2 shows that the SL valence-band edge will evolve completely from within the VCA Γ_{15v} valley, while the conduction-band-edge states could arise from any of the VCA Γ, X, or L conduction-band minima because of the near degeneracy of all these states. Furthermore, these conduction-band states will experience strong intervalley mixing. At $\overline{M}=X^x+X^y$ and $\overline{L}=L_{111}+L_{1\overline{1}\overline{1}}$, this is due to symmetry-forced degeneracies; at $\overline{\Gamma}=\Gamma+X^z$, it is due to an accidental near degeneracy. The resulting SL conduction-band-edge levels are shown in Fig. 6. The $n=1$ SL is found[42] is to be indirect at $\overline{M}$, while for $n=2$ and 3, the direct-indirect energy difference (0.01–0.02 eV) is too small to enable a reliable prediction of the nature of the fundamental gap. The general trend, however, is that of a strong downward bowing from the VCA levels at $n=1$, a negligible shift at $n=2$, and a moderate downward shift at $n=3$. This is in agreement with the general n dependence of intervalley mixing described in Sec. III, where we postulated that intervalley couplings (and their resulting energy-level splittings and repulsions) would be minimal for even n, and would decay like $1/n$ for odd n. We now demonstrate this in detail for the SL levels at each of $\overline{\Gamma}$, $\overline{M}$, and $\overline{L}$.
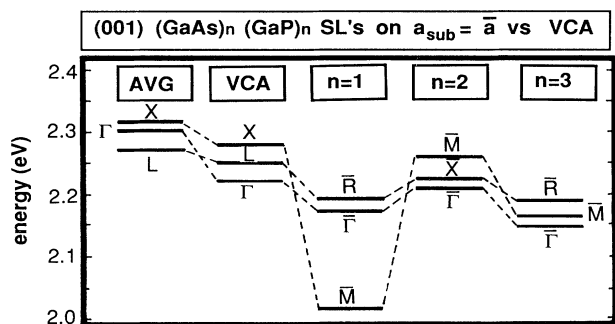
FIG. 6. Conduction-band-minima states of the (001) SL's on $a_{sub}=\overline{a}$, in relation to their parent VCA levels and the average (av) of the equilibrium zinc-blende levels of the GaP and GaAs constituents. All energies (in eV) are with respect to the respective valence-band maxima at Γ or $\overline{\Gamma}$. Note that the dashed lines connecting the states at $k=0$ are not fully significant, since the SL states at $\overline{\Gamma}$ also have varying amounts of X^z character.

1. Valence-band levels at $\overline{\Gamma}$

Figure 7 shows the calculated SL levels at $\overline{\Gamma}$ (neglecting spin-orbit effects), together with the band-offset wells (of the *strained* constituents) that these states exist in. Also shown is the degree of localization of each SL state

in the two halves of its unit cell, and the squared projections of the SL states onto those of their parent VCA compound. Note that the VCA basis is used only to analyze the already calculated (in a very complete plane-wave basis) SL wave functions. The SL levels at $n=3$ were set in relation to the constituent's band-edge levels by the band-offset calculation done for the $n=3$ SL. No such band-offset calculation was done for $n=1$ or 2, however, due to the thin layers involved there. In those cases, we have simply related the SL levels to those of the strained constituents by aligning the $n=1$ and 2 SL valence-band maximum with that at $n=3$. (This same alignment procedure was done in Fig. 5 also.) The smallness of the error involved in this approximation can be seen by considering the valence-band-edge levels shown in Fig. 7. As n increases from 1 to 3, these three valence-band-maxima states develop only a small amount of $\mathbf{k}\neq0$ character, evolving only from 58% to 69% localized in the GaAs well. Being composed almost entirely of the VCA Γ_{15v}, the SL $\bar{\Gamma}_{5v}$ and $\bar{\Gamma}_{3v}$ states remain near the center of the band-offset wells in the $n=3$ calculation [see Fig. 7(c)], falling only slightly down into the GaAs half. Since the degree of localization does not change much between $n=1$ and 3, the resulting error is expected to be small [the $n=1$ $\bar{\Gamma}_{5v}$ state perhaps lying 0.05 eV lower in energy than assumed, putting it more at the center of its well than shown in Fig. 6(a)]. In summary then, because of the involvement of only a *single* VCA

valley, the SL valence-band-maxima states at $\bar{\Gamma}$ evolve qualitatively like Kronig-Penney states. Because of the fairly light mass of the VCA Γ_{15v} dispersion, however, the amount of GaAs localization and the degree to which the SL levels fall from well center are both quite small for $n \leq 3$.

2. Conduction-band levels at $\bar{\Gamma}$

Contrary to this valence-band-edge behavior, Fig. 7 shows that the $\bar{\Gamma}$ *conduction*-band-edge states do, as expected, experience a fair amount of Γ-X^z intervalley mixing. These mixings are controlled by the following selection rules, derived in Appendix B from *point*-group symmetries [that require a symmorphic space group, and thus require a cation (anion) origin for even (odd) n]:

$$\langle \Gamma_{1c} | \delta V | X^z_{3c} \rangle = 0 \tag{13}$$

and

$$\langle X^z_{1c} | \delta V | X^z_{3c} \rangle = 0 . \tag{14}$$

These imply that only the X^z_{1c} VCA state mixes with Γ_{1c}: for odd n only the lower X^z conduction-band-edge state mixes, while for even n it is only the upper state that can mix. (Common-anion systems such as GaAs/AlAs have just the opposite behavior.) For $n=1$ and 2, Fig. 7 shows the $\bar{\Gamma}$ conduction-band-edge states to evolve mainly from
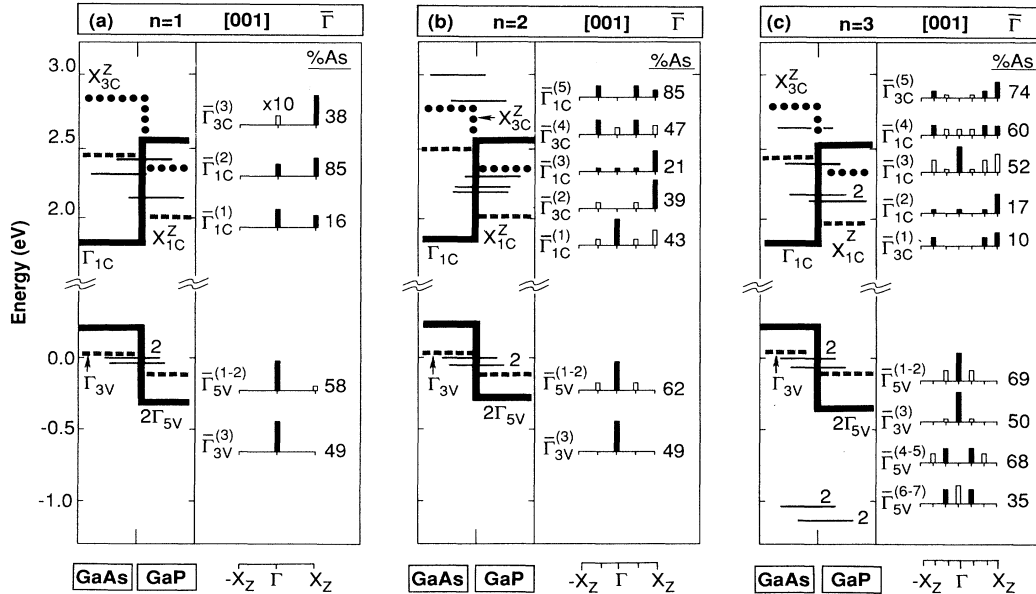
FIG. 7. $\bar{\Gamma}$ levels of the (001) SL's on $a_{sub} = \bar{a}$, together with the corresponding levels of the strained constituents (forming the quantum wells shown in bold lines), their projections onto the VCA parent compound, and the percent of localization into the GaAs half of the SL (labeled %As). The degree of localization is also shown by the centering of the SL levels in their respective quantum wells. Open bars in the VCA decompositions are enhanced by a factor of 10.
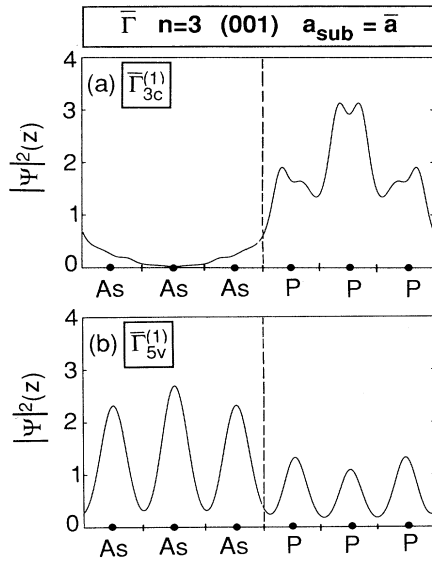
FIG. 8. xy planar average of the squared norm of the conduction-band minimum (a) and valence-band maximum (b) wave functions of the $n=3$ (001) SL at $a_{sub}=\bar{a}$. The planes of Ga atoms are represented by hatches along the abscissa. The dashed vertical line denotes the position of the interface.

functions and in terms of the magnitude of the resulting level repulsion. A nonmonotonic energy versus n behavior is seen in Table I, which is typical of ultrathin period SL's: the $\bar{\Gamma}$ conduction-band minimum has energies 2.17, 2.21, and 2.15 eV for $n=1$, 2, and 3, respectively. By $n=3$, however, the heavy longitudinal X^z mass allows for the SL $\bar{\Gamma}$ minimum to develop from *within* the VCA X^z valley, resulting in two SL states [$\bar{\Gamma}^{(1)}_{3c}$ and $\bar{\Gamma}^{(2)}_{1c}$ in Fig. 7(c)] that Kronig-Penney-localize in the GaP X^z_{1c} well. The wave functions of the conduction-band- and valence-band-edge states of the $n=3$ SL are shown in Fig. 8, which demonstrates the approximate type-II localization behavior resulting from Kronig-Penney-type envelope functions. Note that the degree of localization is much stronger in the conduction-band-edge state, due to the near degeneracy (and thus much stronger intravalley mixing) of the $\pm\frac{2}{3}X^z$ and X^z states involved.

Table I summarizes the calculated transition energies at $\bar{\Gamma}$, and demonstrates the quantitative manner in which these SL energies are related to those of the VCA parent compound: at $n=1$, for example, the two $\bar{\Gamma}_{1c}$ SL levels have an average energy the same as that of their VCA parent levels Γ_{1c} and X^z_{1c}, with the SL energy separation of 0.17 eV having increased from the VCA value of 0.06 eV due to an intervalley coupling strength $U=0.08$ eV [see Eq. (8)].

3. Conduction-band levels at $\bar{M}$

Consider now the SL levels at $\bar{M}$, where the folding $\bar{M}=X^x+X^y$ implies symmetry-forced intervalley mixings between exactly degenerate valleys. Figure 9 shows the SL levels at $\bar{M}$, together with their VCA decompositions

the 2×2 Hamiltonian with off-diagonal element $\langle\Gamma_{1c}|\delta V|X_{1c}\rangle$. According to the discussion of Sec. III, we thus expect strong intervalley mixing at $n=1$, but much weaker mixing at $n=2$. This is indeed seen in Fig. 7, both in terms of the VCA decompositions of SL wave
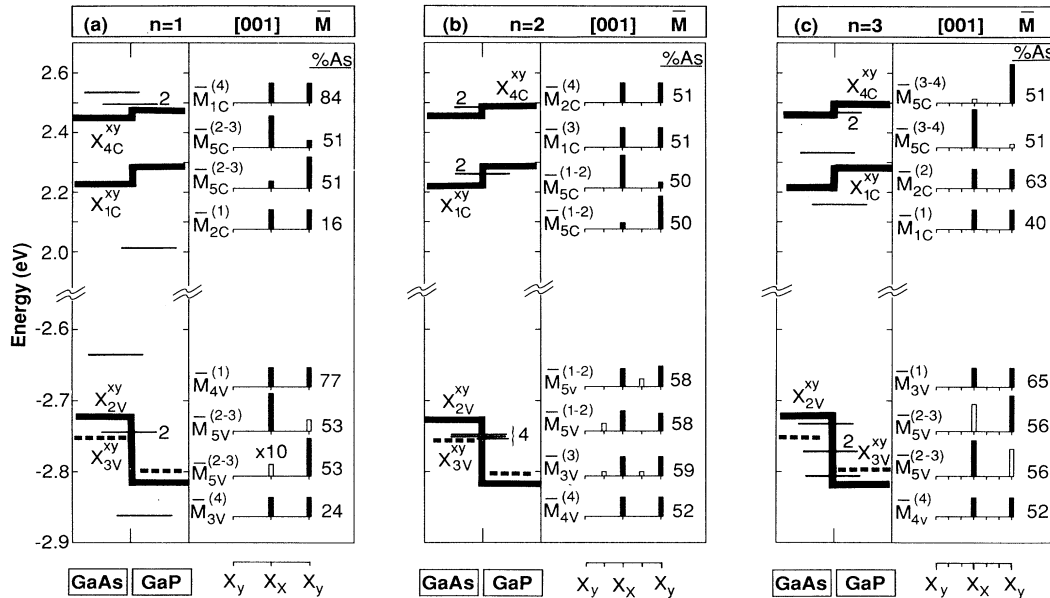
FIG. 9. (001) SL levels at $\bar{M}$. See also Fig. 7 caption.

and the X^{xy} strained constituent band-edge levels. Note from the (001) dispersion of the VCA conduction bands between X^x and X^y shown in Fig. 2(b) that the extremely light transverse X masses suggest the absence of VCA states from $\mathbf{k}$ points between the main X^x and X^y valleys in these SL states for $n \leq 3$. This is indeed seen in the VCA decompositions shown in Fig. 9. This means that the SL conduction-band edge at $\overline{M}$ will consist of four levels, which are made entirely from four VCA levels: the degenerate pair X^x_{1c} and X^y_{1c} and the separate degenerate pair X^x_{3c} and X^y_{3c}. The resulting $\overline{M}$ levels can thus be obtained by diagonalizing the 4×4 Hamiltonian matrix $\langle X^{x/y}_{1c/3c} | \delta V | X^{x/y}_{1c/3c} \rangle$.

As shown in Table II, many elements of this matrix are required to vanish by symmetry. First, there is no mixing between X_{1c} and X_{3c} states in general, splitting the 4×4 matrix into two 2×2 submatrices. Second, the off-diagonal part of the X_{3c} submatrix is required to vanish, meaning that the two X^x_{3c} and X^y_{3c} states remain degenerate (and thus evolve into an $\overline{M}_{5c}$ doublet). Understanding the behavior of the conduction-band levels at $\overline{M}$, shown in Fig. 9, is now straightforward: When n is odd there is an anion origin and the lower conduction-band X^{xy} levels, having X_1 symmetry, split into $\overline{M}_{1c}$ and $\overline{M}_{2c}$, while the upper conduction-band X^{xy} levels, having X_3 symmetry, remain unsplit and become the $\overline{M}_{5c}$ doublet. When n is even, there is a cation origin and the lower conduction-band X^{xy} levels are of X_3 symmetry, thus evolving into the $\overline{M}_{5c}$ doublet, while the upper X^{xy} levels are of X_1 symmetry and can thus split into $\overline{M}_{1c}$ and $\overline{M}_{2c}$. Table I summarizes the calculated conduction-band levels at $\overline{m}$, and shows that the SL levels are positioned exactly as described in Sec. III C: the splittings approximately vanish for even n, while for odd n they decay like $1/n$ (being 0.522 eV at $n = 1$ and 0.174 eV at $n = 3$). The unsplit doublets lie just at the parent VCA energy (the middle position in their respective wells; see Fig. 9), while the levels that do split have their average energy at this midwell position. (At $n = 1$, the $\overline{M}_{5c}$ doublet misses this midwell energy by 0.05 eV due to the approximate positioning of the absolute energy scale there, as was mentioned above.) Furthermore, the spatial localization behavior of the SL states behaves similarly: the unsplit levels are perfectly nonlocalized, while the partial localization of the split levels decays like $1/n$. This behavior has been explained previously by Froyen et al.[50] according to the segregation pattern of the resulting SL states. This is demonstrated pictorially in Fig. 10, where we plot the SL

FIG. 10. xy planar average of the squared norm of the SL wave function made from the equally weighted combination of the lowest VCA conduction-band states at X^x and X^y. Vertical hatches represent planes of Ga atoms, while circles represent anion planes. This same wave function forms the two lowest $\overline{M}$ conduction-band minima of the $n = 1$, 2, and 3 (001) SL's, the only difference in each case being the different identities of the anion planes, which are thus shown below the wave function.

state made from the equally weighted combination of X^x_{1c} and X^y_{1c}. Note that its repeat period of two VCA zinc-blende unit cells is commensurate with even n SL's, where 50% of the wave-function norm exists in each half of the SL unit cell. Similarly, in odd n period SL's, the degree of partial localization is seen to decay like $1/n$ from its maximal $n = 1$ value. The splitting between the even and odd combinations $X^x_{1c} \pm X^y_{1c}$ reflects the disparity in the localization behavior between these two SL states, and will thus have a similar n dependence.

4. Valence-band levels at $\overline{M}$

Consider now the valence-band levels at $\overline{M}$. Figure 9 shows their behavior to be qualitatively similar to that of the conduction-band levels described above. Note from their VCA projections that they evolve almost entirely from the X_{5v} doublets at X^x and X^y, without much involvement of VCA states from intervening $\mathbf{k}$ points (just as in the conduction band). They are thus described by a 4×4 Hamiltonian whose basis states X^x_{5v} and X^y_{5v} are all degenerate. Consideration of selection rules (see Appendix B) gives a matrix with zeros positioned exactly as in Table II. Therefore, two of the four VCA levels remain unsplit (making the $\overline{M}_{5v}$ doublet), while the other two split into $\overline{M}_{3v}$ and $\overline{M}_{4v}$ levels, the magnitude of the splitting behaving just as the conduction band (vanishing at

TABLE II. Hamiltonian matrix $\langle X^{x/y}_{1c/3c} | \delta V | X^{x/y}_{1c/3c} \rangle$ that determines the (001) SL conduction-band-edge levels at $\overline{M}$. The zero entries are the result of symmetry-imposed selection rules, as derived in Appendix B.

	X^x_{1c}	X^y_{1c}	X^x_{3c}	X^y_{3c}
X^x_{1c}	a	b	0	0
X^y_{1c}	b^*	a	0	0
X^x_{3c}	0	0	c	0
X^y_{3c}	0	0	0	c

$n=2$, while being one-third as large at $n=3$ as at $n=1$). The relation of these SL levels to the potential wells formed by the band edges of the strained constituents is just as noted above: the unsplit levels remain at the center of the well, while the split levels maintain their average also at that central position, because the well midpoint is the energy of the degenerate VCA levels from which these SL levels evolve.

5. Levels at $\bar{L}$

The SL levels at $\bar{L}$ are described by a combination of both of the complementary small n resonant level and large n Kronig-Penney pictures. This is expected from the (001) dispersion of the VCA bands between L_{111} and $L_{11\bar{1}}$ shown in Fig. 2(c), which shows two light-mass degenerate valleys forming the $\bar{L}$ conduction-band edge (just at $\bar{M}$), while the SL valence-band edge is seen to evolve from a similar pair of light-mass valleys together with a nearly flat band that will lead to strongly localizing Kronig-Penney states. The midwell centered splitting pattern and its generic n dependence is indeed seen in the calculated $\bar{L}$ conduction band shown in Fig. 11 and Table I. [The 0.05-eV error in the positioning of the absolute energy scale for $n=1$ is apparent in Fig. 11(a).] Note the VCA decompositions there show the absence of involvement of VCA states from between the main two valleys, leading to the resonant character of the states shown.

The $\bar{L}$ valence-band levels in Fig. 11 show the existence of two resonant-type levels at the center of the potential well whose splittings behave as predicted and whose VCA projections show only L_{111} and $L_{11\bar{1}}$ contributions. Together with these states is another set of Kronig-Penney-type levels whose VCA decomposition shows them to be

composed of the flat-band VCA states of neighboring $\mathbf{k}$ (with *minimal* $\delta\mathbf{k}$), thus allowing them to localize their wave functions nearly completely in the alternate halves of the SL, and causing their energy levels to lie at the extremes of the I_{2v} well (i.e., just at the energies of the strained constituents, apart from a small amount of confinement energy). The nearly infinite (001) L_{111} mass explains the observation of Recio *et al.*[32] that the E_1 and $E_1+\Delta_1$ transitions show much less quantum confinement than the near-band-gap transitions. The separation of the SL levels into nonlocalizing (resonant) levels evolving from two degenerate light-mass states and localizing (Kronig-Penney) levels arising from a nearly flat band has its origin in the symmetry-imposed block diagonal form of the pertinent Hamiltonian matrix $\langle \psi_{\mathbf{k}'\alpha'}|\delta V|\psi_{\mathbf{k}\alpha}\rangle$. As shown in Appendix B, one state of the L_{3v} doublet of the VCA zinc blende is prohibited by symmetry to mix with either its same-$\mathbf{k}$ degenerate partner or with any of the flat-band states at intervening $\mathbf{k}$ between L_{111} and $L_{11\bar{1}}$. A 2×2 subblock of the Hamiltonian matrix is formed by one such state from each of L_{111} and $L_{11\bar{1}}$, giving rise to the resonant $\bar{L}_{1v}$ and $\bar{L}_{3v}$ SL levels that lie at the center of the potential well. The rest of the Hamiltonian matrix is of like symmetry and mixes completely (due to the vanishing energy denominators), giving rise to the $\bar{L}_{2v}$ and $\bar{L}_{4v}$ Kronig-Penney-type levels described above.

The envelope-function nature of these Kronig-Penney-type levels is shown in Fig. 12. There we plot the xy planar average of the squared norm of the top three SL valence-band states of the $n=3$ SL at $\bar{L}$, labeled $\bar{R}_{4v}^{(1)}$, $\bar{R}_{2v}^{(2)}$, and $\bar{R}_{4v}^{(3)}$ in Fig. 11(c). As shown there, these states lie, apart from a small amount of confinement energy, at the bottom of the I_{2v} GaAs potential well. Their VCA projections show them to be composed of neighboring
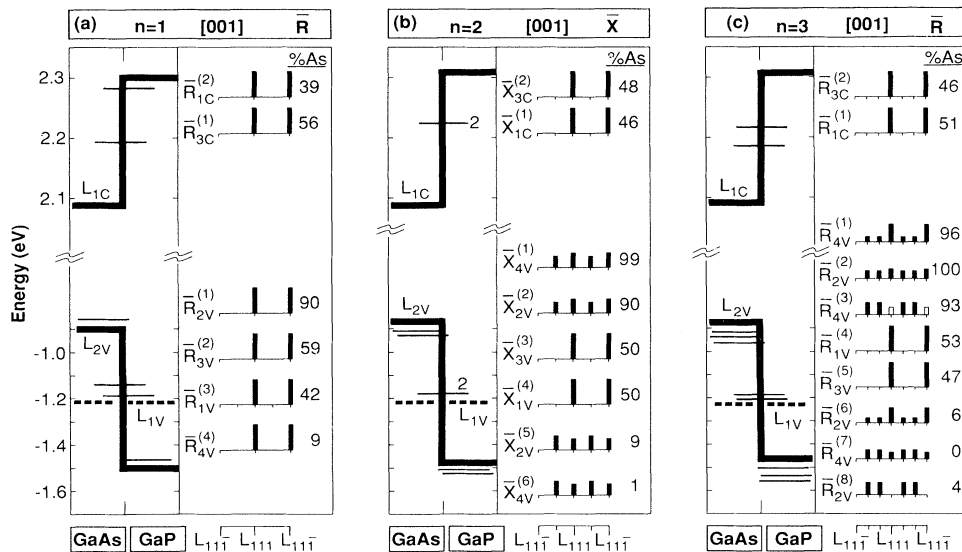
FIG. 11. (001) SL levels at $\bar{L}$. See also Fig. 7 caption.
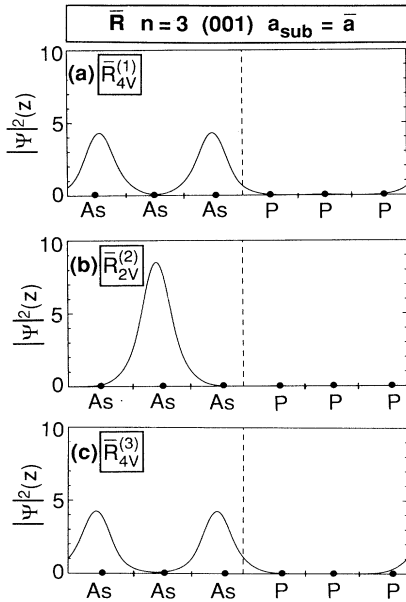
FIG. 12. xy planar average of the squared norm of the top three valence-band wave functions of the $n=3$ (001) SL at $\bar{R}$. Note the extreme GaAs localization, due to the nearly infinite mass of the (001) L_{111}-$L_{11\bar{1}}$ dispersion. Note also that the usual Kronig-Penney ground-state envelope function (being nodeless) is now just the second lowest level, while the first and third states arise from even and odd single-node envelope functions, due to the intervalley mixing.

zinc-blende states with minimal δk, resulting in their being 96%, 100%, and 93% localized in the GaAs half of the SL, respectively. The reason such extreme Kronig-Penney-type behavior is seen even in these ultrathin $n=1-3$ systems here is because of the near-infinite mass of the band involved, resulting in near-vanishing energy denominators. The wave-function plots of Fig. 12 show the extreme GaAs localization of these states, but also demonstrate a manner in which they do not behave as typical *single-valley* Kronig-Penney states. This new behavior, due to *two* interacting heavy-mass valleys, is simply that the usual Kronig-Penney ground state (having a nodeless envelope function) is now just the second-lowest SL state $\bar{R}_{2v}^{(2)}$, whereas the first- and third-lowest SL levels $\bar{R}_{4v}^{(1)}$ and $\bar{R}_{4v}^{(3)}$ arise from a splitting of two states that, in the Kronig-Penney sense, would be first excited states (having one node in their envelope functions). This is in contrast to the typical singley-valley behavior of the $\bar{\Gamma}$ band-edge states shown in Fig. 8.

6. Comparison to GaAs/AlAs

It is instructive to compare these present results on $(GaP)_n(GaAs)_n$ SL's to similar results on the $(AlAs)_n(GaAs)_n$ system. There are three reasons for this.

First, as was mentioned in the Introduction, there is a significant amount of published work on this system (both experimental and theoretical), and application of the principles enunciated above will clarify some of the established (and debated) results. Second, this comparison will demonstrate some important generic differences between common-anion and common-cation systems. Third, the brief application of the present theory to AlAs/GaAs serves both as a further exercise in its implementation and as a further demonstration of its usefulness.

For these reasons we show in Table III, in exact analogy with Table I, the energies of (001) $(AlAs)_n(GaAs)_n$ SL states in relation to the energies of their parent VCA levels. These SL levels were calculated by the same methods used above for GaP/GaAs. Note that although the minimum conduction-band level in the VCA compound is at X (by over 0.14 eV), the conduction-band minimum of the SL is calculated to be at $\bar{L}$ at $n=1$ and at $\bar{\Gamma}$ or $\bar{M}$ at $n=2$ and 3 (the $\bar{\Gamma}$-$\bar{M}$ difference of less than 0.03 eV in these latter two cases being smaller than our calculational uncertainty). These results are in agreement with those of previous self-consistent calculations.[11,22,63] This behavior can be understood as follows. First, note that the splittings $\Delta\varepsilon$ at $\bar{M}$ and $\bar{L}$ have the exact n dependence we have predicted, and that the average of the split levels lies at approximately the same energy as the VCA parent level. Note, however, how the selection rules have been reversed compared to the common-anion GaP/GaAs case, due to the fact that even (odd) N systems now require an anion (cation) origin to keep the space-group symmorphic. At $\bar{M}$, this means that for odd n the lower conduction-band X^{xy} levels remains unsplit (forming the $\bar{M}_{5c}$ doublet), while the upper X^{xy} levels split strongly there into $\bar{M}_{1c}$ and $\bar{M}_{2c}$. As has been noted elsewhere,[8] this is in agreement with other semiempirical calculations[19,44] that find the opposite result. Note further that at $n=1$ this explains why the conduction-band minimum does not occur at $\bar{M}$ as it does in GaP/GaAs. Rather, in spite of the fact that the VCA conduction-band minimum occurs at X, the SL minimum occurs at $\bar{L}$, there being a huge splitting of 0.96 eV there (similar in size to the 0.91-eV splitting of the upper X^{xy} conduction-band level at $\bar{M}$). The much greater magnitude of these splittings as compared to the corresponding ones in GaP/GaAs (0.52 and 0.09 eV, respectively; see Table I) is the other major generic difference between common-cation and common-anion systems. It can be explained by noting that, for a lattice-matched system like AlAs/GaAs, the SL ordering perturbation is mainly an s-like function centered about the noncommon atoms. (The s character results from the difference in the bare nonlocal pseudopotentials lying mainly in their s components.[52]) The zinc-blende L_{1c} conduction-band state is mainly cation s-like (with a smaller amount of anion-s and -p character). The lower zinc-blende X conduction-band state is anion-s plus cation-p, while the upper state is the reverse (cation-s plus anion-p).[51] This means that in a common-anion system like AlAs/GaAs, L_{1c} and the upper X^{xy} conduction-band state will couple strongly to the SL ordering potential δV, causing a large energy splitting. For a common-cation

TABLE III. Principal conduction-band edges of the $(AlAs)_n(GaAs)_n$ (001) SL's, in relation to their parent VCA levels. In the cases of $\overline{M}$ and $\overline{L}$, $\Delta\varepsilon$ is the splitting of the two degenerate VCA levels that fold there. All energies are in eV, and are measured with respect to the respective valence-band-maximum state at Γ or $\overline{\Gamma}$, including spin-orbit effects. The asterisk in each column denotes the conduction-band minimum. A gap correction of 0.92 eV was added to all calculated conduction-band energies here. Note that the levels here differ slightly from those calculated in Ref. 22 (by less than 0.10 eV) and from those in Ref. 11 (by less than 0.14 eV) due to the different gap corrections performed in each case. (The states labeled $\overline{\Gamma}_{3c}$, $\overline{M}_{3c}$, and $\overline{R}_{3c}$ here were labeled Γ_{4c}, $\overline{M}_{4c}$, and $\overline{R}_{4c}$ in those two references.)

Origin	VCA Anion	$n=1$ Cation	$n=2$ Anion	$n=3$ Cation
Γ	$X^z_{1c}=2.14^*$	$\Gamma_{1c}=2.06$	$\overline{\Gamma}_{1c}=2.09^*$	$\Gamma_{3c}=2.05^*$
	$\Gamma_{1c}=2.28$	$\overline{\Gamma}_{3c}=2.22$	$\overline{\Gamma}_{1c}=2.21$	$\overline{\Gamma}_{1c}=2.15$
	$X^z_{3c}=2.71$	$\overline{\Gamma}_{1c}=2.97$	$\overline{\Gamma}_{3c}=2.65$	$\overline{\Gamma}_{1c}=2.48$
$\overline{M}$	$X^{xy}_{1c}=2.14^*$	$2\overline{M}_{5c}=2.16$	$\overline{M}_{2c}=2.12$ $\overline{M}_{1c}=2.15$	$2\overline{M}_{5c}=2.08$
	$X^{xy}_{3c}=2.71$	$\overline{M}_{1c}=2.27$ $\overline{M}_{2c}=2.18$	$2\overline{M}_{5c}=2.70$	$\overline{M}_{1c}=2.53$ $\overline{M}_{2c}=2.83$
$\Delta\varepsilon$		0.905	0.031	0.296
$\overline{L}$	$L^{111}_{1c}=2.39$	$\overline{R}_{1c}=1.95^*$	$\overline{X}_{1c}=2.35$	$\overline{R}_{1c}=2.19$
	$L^{111}_{1c}=2.39$	$\overline{R}_{3c}=2.91$	$\overline{X}_{3c}=2.37$	$\overline{R}_{3c}=2.49$
$\Delta\varepsilon$		0.961	0.027	0.301

system like GaP/GaAs, however, the chemical part of the SL ordering potential, δV_{chem}, is anion centered, and the strain piece δV_{str} due to the lattice mismatch adds p_z character to δV. This results in a much smaller splitting at L_{1c}, while the X^{xy} state that does split (the lower one now) splits only half as much as in AlAs/GaAs (because its anion-s character is only half of the cation-s character of the upper X^{xy} state, which splits in the common-anion case). These arguments are very approximate, and are meant only to suggest a probable connection between the orbital character of various states and their resulting splittings in common-anion or common-cation SL ordering.

At $\overline{\Gamma}$, Table III shows that the three lowest SL conduction-band levels evolve straightforwardly from the three VCA states Γ_{1c}, X^z_{1c}, and X^z_{3c} for $n=1$ and 2, just as in GaP/GaAs, except that the dependence of the Γ-X^z mixings on even versus odd n is now reversed. For example, at $n=1$, the $\overline{\Gamma}_{3c}$ level is just the lower VCA conduction-band X^z level, while the two Γ_{1c} states result from mixing the VCA Γ_{1c} and upper X^z states. Note that the average energy of the two SL levels is just the average energy of the two component VCA levels, while the widening of the energy difference from $\Delta\varepsilon^0 = 2.71 - 2.28 = 0.43$ eV to $\Delta\varepsilon = 2.97 - 2.06 = 0.91$ eV in going from VCA to SL states is due to a large intervalley coupling strength $U=0.40$ eV [see Eq. (8)]. This strong interaction between two VCA states that are 0.43 eV apart, which results in significant oscillator strength sharing [the lower (upper) $\overline{\Gamma}_{1c}$ state being a 70:30 (30:70) mixture of the VCA Γ_{1c} and upper X^z states], is due to

the strong coupling between the large cation-s character of these states and the cation centered SL ordering potential. At $n=2$, the SL $\overline{\Gamma}_{3c}$ state is just the upper VCA X^z state, while the two $\overline{\Gamma}_{1c}$ levels now evolve mainly from the VCA Γ_{1c} and lower X^z states (with negligible level repulsion between the two states due to the even n period). At $n=3$, the $\overline{\Gamma}_{3c}$ state is mainly the lower VCA X^z level (just as for $n=1$). Unlike at $n=1$, however, it is now the lowest $\overline{\Gamma}$ level, because the strong intervalley mixing between the VCA Γ_{1c} and upper X^z states, and its commensurately large level repulsion, is now only one-third as strong. In general, the strong intervalley coupling in this common-anion system is seen by the large $n=1$ intervalley matrix elements U, equal [from Eq. (8)] to 0.40, 0.45, and 0.48 eV at $\overline{\Gamma}$, $\overline{M}$, and $\overline{L}$, respectively, while for GaAs/GaP the corresponding values (0.08, 0.26, and 0.04 eV) are much smaller. In summary, comparison of the GaP/GaAs and AlAs/GaAs systems has verified the characteristic n dependence to the intervalley mixings, and has demonstrated some generic differences between common-cation and common-anion SL's.

V. RESULTS FOR (111) SUPERLATTICES

In this section we present the results for the structural properties, band offsets, and SL electronic levels for (111) $(GaP)_n(GaAs)_n$ SL's, with $n=1$, 2, and 3. Having considered these subjects in great detail for the (001) SL's in the preceding section, we concentrate here mainly on the differences between [111] and [001] growth directions.

A. Structural properties

The nuclear coordinates in the (111) SL's are determined by a method analogous to that used for the (001) systems. We again consider the SL in its bulk equilibrium configuration: its lattice constant $a_\perp$ perpendicular to (111) is assumed to be equal to the average $\bar{a}$ of the lattice constants of the GaP and GaAs zinc-blende equilibrium structures, since we are again only considering equal-period systems. A first guess at the nuclear coordinates within the SL is then obtained by first finding the equilibrium structures of the strained binary compounds (epitaxially constrained to $a_\perp = \bar{a}$), and then layering these strained binaries along [111] to form a SL. Calculation of the self-consistent Hellmann-Feynman forces on the nuclei in the SL then allows for any correction to the cell interval degrees of freedom, while analysis of the stress on the SL unit cell similarly prescribes whether any further [111] unit-cell distortion need be introduced. In the present case, both of these checks implied that no further relaxation of nuclear coordinates was required, and as in the (001) case, the SL was exactly made simply of layers of strained binary constituents [the common Ga atom and the polar nature of (111) atomic planes making such a construction possible].

The nuclear coordinates of the strained binaries were found as follows. After imposition of the epitaxial constraint $a_\perp = \bar{a}$, there are two degrees of freedom left determining the structure of these binary compounds. One is the lattice constant a_{111} of the unit cell in the [111] direction, which we shall describe by a trigonal distortion parameter $\eta = a_{111}/a_\perp$. The other is a cell internal degree of freedom ζ that describes the relative position of the two atoms in the unit cell, their separation being given by the vector $(\zeta,\zeta,\zeta)a_\perp/4$. Minimizing the total energy of the binary compounds with respect to η and ζ (with $a_\perp = \bar{a}$ fixed) gives, for GaAs, $\eta = 1.032$ and $\zeta = 1.024$, while for GaP we obtain $\eta = 0.978$ and $\zeta = 0.986$. Note that since the two η values average 1.005, there is [unlike in the (001) case] a very small (0.5%) overall distortion of the SL unit cell along the growth direction. In summary, the η and $a_\perp$ values given here completely determine the strain configurations of the elastically deformed GaP and GaAs constituents of these (111) SL's.

B. Band offsets

In this section we present the results of our first-principles calculation of the valence-band offsets of the coherent (111) GaP/GaAs interface. As in the (001) case, the bands of the strained binary constituents are put on a common energy scale by a straightforward analysis[40] of the self-consistent charge density of the $n = 3$ SL.

We begin by reporting the valence-band offsets of the strained constituents neglecting spin-orbit effects. In that case, the triply degenerate Γ_{15v} valence-band maximum of the equilibrium zinc-blende compounds is split by the noncubic crystal field into a Γ_{3v} doublet and a Γ_{1v} singlet in the strained binaries. [The point group of the strained binaries, and that of all the (111) $(GaP)_n(GaAs)_n$ SL's, is $C_{3v}(3m)$.] Aligning these states by the method men-

tioned above results in the following energies (all in eV): for GaAs, $\Gamma_{3v} = 0$ and $\Gamma_{1v} = -0.24$, while for GaP, $\Gamma_{3v} = -0.57$ and $\Gamma_{1v} = -0.42$. As in the case of the (001) interface, the GaAs forms the quantum wells while the GaP forms the barriers. The SL valence-band-maxima states will thus be localized to the GaAs region.

We introduce spin-orbit effects using the quasicubic model[55] described in Sec. IV B. The resulting levels of the strained GaP and GaAs are shown in Fig. 13. Together with these calculated valence-band offsets shown are conduction-band offsets obtained by shifting the calculated conduction-band levels by a state-dependent gap correction that is the same as that needed to fix the calculated zinc-blende equilibrium levels to their experimental values. The resulting offsets are very similar to their values for the (001) SL: the valence-band offset is 0.52 eV between the GaAs heavy-hole and GaP upper light-hole plus spin-split state [(001) value was 0.44 eV] while the conduction-band offset is 0.16 eV between the GaAs Γ and GaP X conduction-band minima [(001) value was 0.09 eV]. Note also that the noncubic crystal field due to the trigonal shear component of the strain splits the fourfold point-group degeneracy of the zinc-blende L states into a threefold-degenerate set of states (at $L_{\bar{1}11}$, $L_{1\bar{1}1}$,
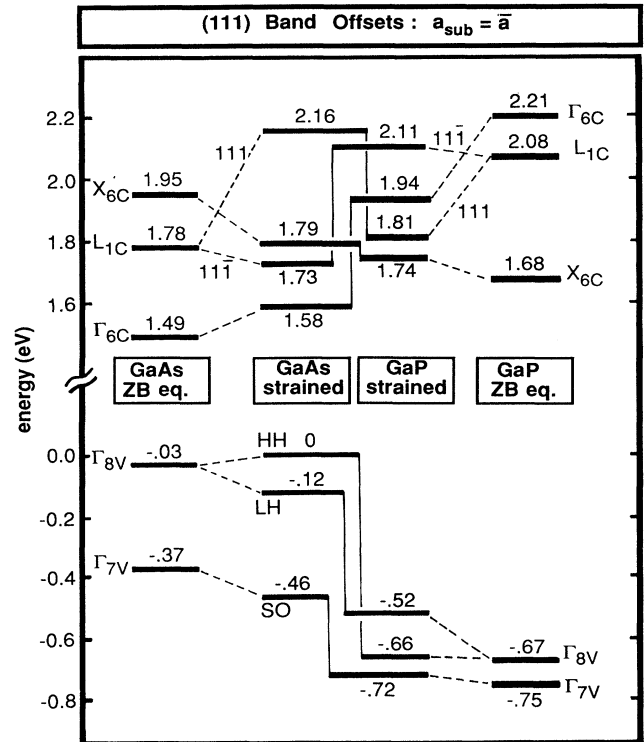
FIG. 13. Calculated band offsets of the (111) GaAs/GaP coherent interface, for the strain conditions appropriate to equal-period SL's (i.e., $a_\perp = \bar{a}$). The offsets of the unstrained constituents are obtained from these strained binary offsets through the absolute deformation-potential model of Ref. 60, which is used only to line up the valence-band maxima at Γ.

ROBERT G. DANDREA AND ALEX ZUNGER

TABLE IV. Principal conduction-band edges of the $(GaP)_n(GaAs)_n$ (111) SL's, in relation to their parent VCA levels. All energies are in eV, and are measured with respect to the respective valence-band-maximum state at Γ or $\overline{\Gamma}$, neglecting spin-orbit effects. (These can be included by subtracting 0.07 eV from all energies here.) The asterisk in each column denotes the conduction-band minimum. A gap correction of 0.85 eV was added to all calculated conduction-band energies here. [Note that in our previous study of the $n=1$ SL (Ref. 42), a shift of only 0.75 eV was applied to the same values. The results in this table are thus 0.1 eV larger than those in Ref. 42.]

	VCA	$n=1$	$n=2$	$n=3$
$\overline{\Gamma}$	$\Gamma_{1c}=2.22^*$	$\overline{\Gamma}_{1c}=2.12$	$\overline{\Gamma}_{1c}=2.09^*$	$\overline{\Gamma}_{1c}=2.02^*$
	$L_{1c}=2.25$	$\overline{\Gamma}_{1c}=2.22$	$\overline{\Gamma}_{1c}=2.12$	$\overline{\Gamma}_{1c}=2.05$
$\overline{X}$	$L_{1c}=2.25$	$\overline{X}_{1c}=2.08^*$	$\overline{X}_{1c}=2.12$	$\overline{M}_{1c}=2.06$
	$X_{1c}=2.28$	$\overline{X}_{1c}=2.24$	$\overline{X}_{1c}=2.17$	$\overline{M}_{1c}=2.11$
	$X_{3c}=2.52$	$\overline{X}_{1c}=2.49$	$\overline{X}_{1c}=2.36$	$\overline{M}_{1c}=2.29$

and $L_{11\overline{1}}$) plus a separate state at L_{111}. The threefold point-group degeneracy of the zinc-blende X states remains, however (i.e., $X^x=X^y=X^z$), unlike in the (001) case. As with the (001) offsets presented earlier, we also show the offsets for the unstrained zinc-blende equilibrium compounds by using an approximate absolute deformation-potential model.[60] The results are again quite similar to the (001) offsets, being 0.64 and 0.19 eV in the valence and conduction bands, respectively. [The (001) values were, respectively, 0.56 and 0.27 eV.]

C. Superlattice energy levels

We now present the analysis of the single-particle electronic energy levels of the (111) SL's. These calculated energies, and those of their VCA parent levels, are sum-

marized in Table IV.

Consider first the folding relationship appropriate to these (111) SL's. As shown in Fig. 14, the Brillouin zone of the $n=1$ and 2 (111) SL's is simple trigonal, while that of the $n=3$ SL is simple hexagonal. From the coordinates of the SL k points shown there, we see that the three major band edges of the VCA parent structure (Γ, X, and L) are folded to just two points of the SL zone. If we generalize the definition of the $\overline{X}$ point to coincide with the $\overline{M}$ point of the $n=3$ zone, then the simple result is that the VCA Γ and $L_{11\overline{1}}$ points are folded to the SL $\overline{\Gamma}$ point, while the VCA X^z and L_{111} points are folded to $\overline{X}$ in the SL zone (two other equivalent $\overline{X}$ points result from the folding of the other two VCA X and L points). Including the intermediate k points along the (111) adjoining line between the two main valleys (which are involved in the folding when $n \geq 2$) gives the following relationships:

$$\overline{\Gamma}= \sum_{j=-n+1}^{n} \Gamma + \frac{j}{n}L_{111}+\Gamma+L_{111}+ \cdots , \quad (15)$$
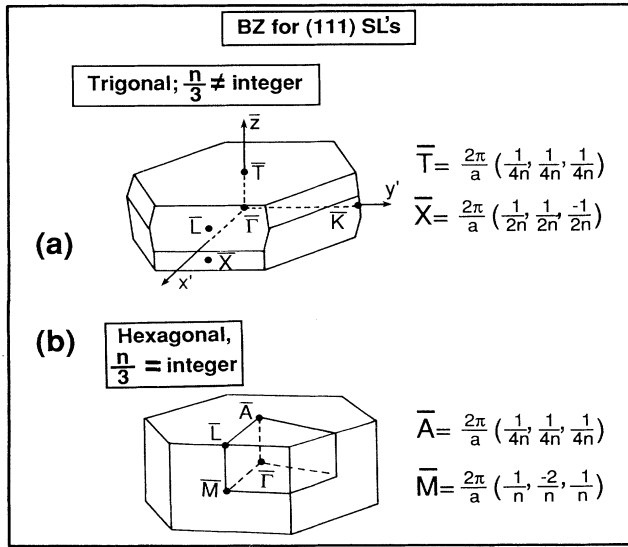
FIG. 14. Brillouin zone of the (111) $(GaP)_n(GaAs)_n$ SL's. (a) Simple trigonal zone for the case of n not being a multiple of 3. The z' axis is along the [111] direction. (b) Simple hexagonal zone for the case of n being a multiple of 3.
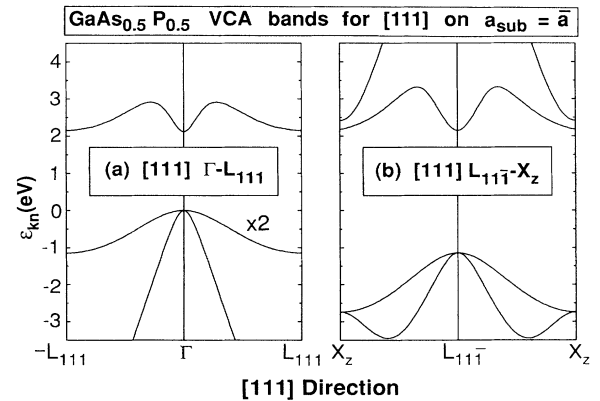
FIG. 15. Bands of the VCA Ga⟨AsP⟩ zinc-blende compound along the (111) lines between the principal band-edge valleys. The bands in (a) are folded to $\overline{\Gamma}$ in the SL zone, while those in (b) are folded to $\overline{X}$ (for $n=1$ and 2) and to $\overline{M}$ for $N=3$.

$$\overline{X} = \sum_{j=-n+1}^{n} X^z + \frac{j}{n} L_{111} = X^z + L_{111} + \cdots . \qquad (16)$$

Figure 15 shows the (111) dispersion of the VCA bands between the main band-edge valleys. Figure 15(a) shows the states that are folded to $\overline{\Gamma}$ in the SL, while Fig. 15(b) shows the VCA states folded to $\overline{X}$. From the analysis of Sec. III, the following general observations can be made simply from these VCA band plots. First, consider the top valence bands in Fig. 15. They both show only one valley being involved (the VCA Γ for $\overline{\Gamma}$, and the VCA $L_{11\overline{1}}$ for $\overline{X}$), and are thus expected to give rise only to standard Kronig-Penney-type SL states. The Γ-L_{111} dispersion of about 1 eV is only one-third of the (001) Γ-X^z dispersion shown in Fig. 2(a). We thus expect the (111) $\overline{\Gamma}$ valence-band-edge states to localize in their GaAs well much faster than they did for (001), due to the heavier mass now involved. Consideration of the conduction bands in Fig. 15, however, suggests that there might be strong intervalley mixing both at $\overline{\Gamma}$ and at $\overline{X}$, due to the nearness in energy of all three of the main VCA conduction-band valleys. We thus do not expect to see there the typical Kronig-Penney-type behavior that is expected in the SL valence-band-edge states.

Figures 16 and 17 show the SL states at $\overline{\Gamma}$ and at $\overline{X}$, together with their VCA decomposition, degree of localization, and position with respect to the pertinent band-edge levels of the strained GaP and GaAs constituents. Note that the SL valence-band-maxima states behave just as predicted above: they are typical single-valley Kronig-Penney states that localize in their respective GaAs wells. Because the (111) VCA Γ mass is heavier than its (001) counterpart, the $n=3$ valence-band-maximum wave function at $\overline{\Gamma}$ is much more GaAs localized than in the (001)

case (86% versus 69%), and its energy level has fallen farther down into the GaAs well from its starting position at the well center. Note that, as in the (001) case, the SL levels are accurately put on a common energy scale with the band-edge levels of the strained constituents (which form the wells and barriers) only for the $n=3$ case, where a band-offset calculation is performed. For $n=1$ and 2, however, these levels were positioned on this absolute energy scale simply by aligning the SL valence-band maxima at $\overline{\Gamma}$. The error involved in this approximation is clear in Figs. 16 and 17: at $n=1$ the SL levels are almost entirely composed of a single VCA state, and should thus sit at the center of their respective potential wells, which is about 0.1 eV lower in energy than they are positioned in these two figures. (This is also seen in Table IV, where the average energy of the two lowest $n=1$ $\overline{\Gamma}$ levels is 0.07 eV lower than the average of their VCA Γ_{1c} and $L_{111,1c}$ parent states, when a common zero-energy valence-band maximum is assumed.)

Figures 16 and 17 show that the SL conduction-band-edge states at $\overline{\Gamma}$ and $\overline{X}$ indeed show a fair amount of intervalley mixing, as expected. However, because of the common-cation nature of GaAs/GaP, the resulting level repulsion is small. For example, Table IV shows that the VCA Γ_{1c} and $L_{111,1c}$ states involved in the SL states at $\overline{\Gamma}$ have an energy difference $\Delta\varepsilon^0 = 0.03$ eV, while the two $n=1$ SL states are split only by $\Delta\varepsilon = 0.10$ eV, due to a very small intervalley coupling strength $U=0.05$ eV [see Eq. (8)]. Furthermore, note that the smallness of $\Delta\varepsilon^0$ leads to a fair amount of wave-function mixing even in the $n=2$ SL at $\overline{\Gamma}$. The argument given in Appendix A explains why the magnitude of U should be small for even n. However, the translation of this principle into one of much weaker wave-function mixing for even N relies on
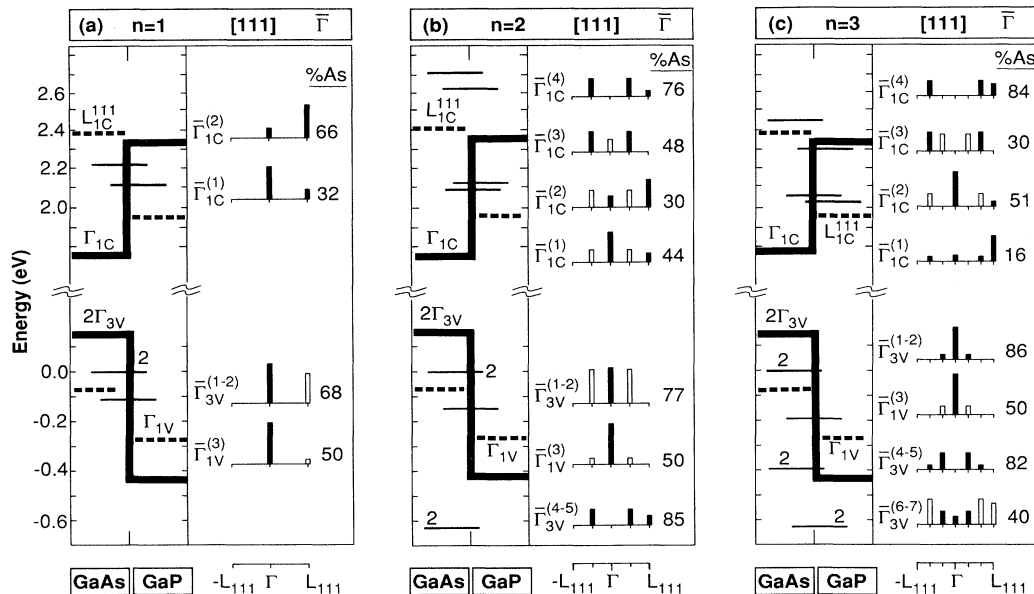
FIG. 16. (111) SL levels at $\overline{\Gamma}$. See also Fig. 7 caption.
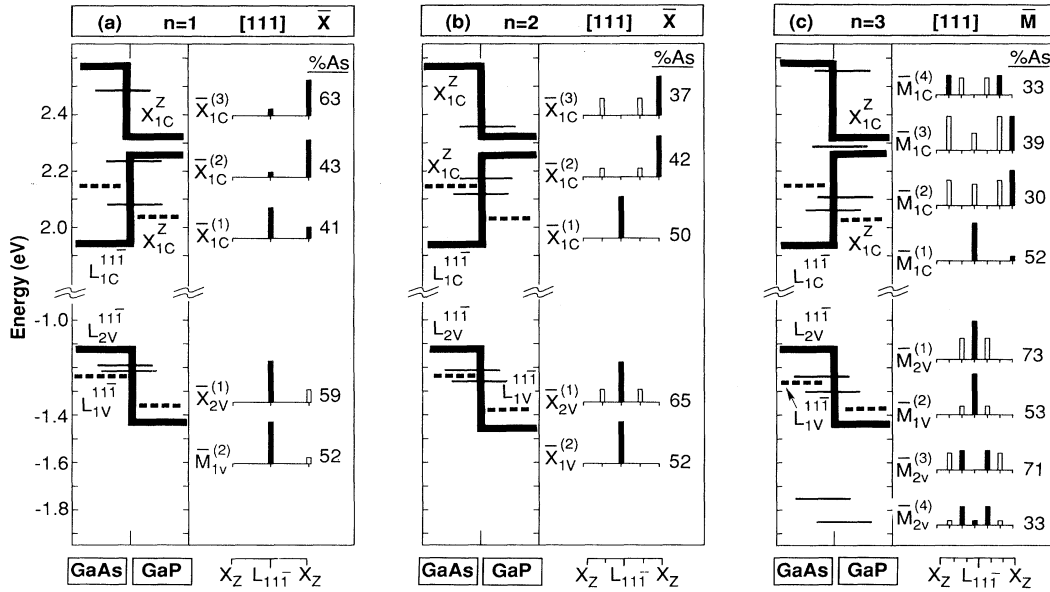
FIG. 17. (111) SL levels at $\overline{X}$. See also Fig. 7 caption.

the resulting U value being smaller than $2\Delta\varepsilon^0$. [See the discussion following Eq. (8).] In the present case, the original VCA splitting $\Delta\varepsilon^0$ is so small that there remains at $n=2$ a fair amount of wave-function mixing, even though the level repulsion (controlled by the size of U) is still quite small. By $n=3$ the heavy-mass VCA L_{111} conduction-band valley leads to a SL conduction-band-edge state made from *intra*valley mixing within this VCA valley, which is thus localized in the GaP L_{1c} well. Similar behavior holds for the conduction-band states at $\overline{X}$, due to the similarity of their parent VCA bands with those involved at $\overline{\Gamma}$ [compare Figs. 15(a) and 15(b)].

Comparison to the GaAs/AlAs system is again worthwhile: Table III shows that the VCA $\langle\text{AlGa}\rangle\text{As}$ L_{1c} and Γ_{1c} states are split by $\Delta\varepsilon^0 = 2.39 - 2.28 = 0.11$ eV. Our calculations at $n=1$ show two SL states at 1.86 and 2.86 eV.[64] Their average energy is at the average of the component VCA energies, while the large level repulsion (compare $\Delta\varepsilon = 1.00$ eV to $\Delta\varepsilon^0 = 0.11$ eV) is due to a large intervalley matrix element $U = 0.50$ eV, as expected in this common-anion system. The VCA decompositions of these SL states show them to be made of 50:50 mixtures of the Γ_{1c} and L_{1c} states. At $n=2$, however, we find two SL $\overline{\Gamma}$ states at 2.01 and 2.18 eV, showing much less level repulsion. The VCA decompositions of these states show them to have almost zero mixing of Γ_{1c} and L_{1c}, as expected from our general theory in the case $2U < \Delta\varepsilon^0$.

Summarizing, in the (111) SL's the three main VCA band edges at Γ, X, and L are folded to just two SL points, $\overline{\Gamma}$ and $\overline{X}$. The main difference between these folding relationships and those of (001) SL's is that there is, in the present (111) case, no intervalley mixing of degenerate states as there was at $\overline{M}$ and $\overline{L}$ in the (001) case. This results in the SL valence-band-edge states having as

typical single-valley Kronig-Penney states, localizing into their respective GaAs wells, while the SL conduction-band-edge states experience some intervalley mixing due to the nearness in energy of the corresponding VCA parent levels. By $n=3$, however, the conduction-band edge at $\overline{\Gamma}$ does localize into the GaP L_{1c} well, giving rise to a type-II SL. Consideration of the band offsets shown in Figs. 13 or 16 thus predicts a type-II–to–type-I transition to occur for sufficiently large repeat period n, in exact analogy with the well-known (001) GaAs/AlAs example. Note that the calculated SL conduction-band minima at both $\overline{\Gamma}$ and $\overline{X}$ all lie, for $n=1$, 2, and 3, within the energy range 1.9–2.0 eV, with the direct-indirect energy difference being less than 0.05 eV. We are thus unable to predict the nature of the absolute conduction-band-minimum state in these (111) SL's, because such small energy differences are beyond the present calculational uncertainty.

VI. [110] AND [201] GROWTH DIRECTIONS

Although the [001] and [111] directions are the most popular for SL growth, SL's are occasionally grown (and sometimes spontaneously order[14(a)]) in the [110] and [201] directions also. For this reason, we present in this section the following relationships that determine the SL levels in [110] and [201] systems. We present no actual calculations of such SL's. Rather, we simply show the VCA bands that determine the SL levels in these systems, and employ the model of Sec. III to predict the character of the resulting SL states.

Consider first the (110) SL's. A SL state at a given point $\mathbf{k}$ in the SL zone will be composed of VCA zinc-blende states along the line $\mathbf{k}\pm(2\pi/a)(1,1,0)=\mathbf{k}\pm\frac{4}{3}K_{110}$. Consideration of the point-group symmetry of the (110)

SL then yields the following result: the three main band edges of the parent zinc-blende compound (Γ, X, and L) are folded to four points in the SL zone. The resulting folding relationships, shown in Fig. 18, are similar to those of (001) SL's, except for the fact that there are now two inequivalent $\overline{\Gamma}$ points. In particular, the VCA Γ and X^z points are folded on top of each other, as are X^x and X^y, L_{111} and $L_{11\overline{1}}$ (which fold to $\overline{L}$), and $L_{\overline{1}11}$ and $L_{1\overline{1}1}$ (which fold to $\overline{L}'$). Consideration of the band dispersions along the (110) lines adjoining these two main valleys then suggests the following behavior for the resulting SL states: The zone-center SL states will behave much like in the (001) case, except for the fact that the lighter (110) X^z_{1c} mass [in comparison to the heavy longitudinal mass; compare Figs. 18(a) and 2(a)] will delay the onset of localization into the GaP X^z conduction-band well, while the heavier (110) Γ_{15v} mass will accelerate the localization into the GaAs Γ valence-band well.

Comparison of Figs. 18(b) and 2(b) shows that the (110) SL conduction-band states made from the X^x-X^y folding will be nearly identical to those for (001), showing typical well-centered resonant behavior due to intervalley mixing between two degenerate light-mass valleys. In particular, for even n, SL doublet states will exist nearly exactly at the energy of the VCA X^{xy}_{1c} and X^{xy}_{3c} conduction-band states (i.e., at their well centers); for odd n, there will exist a splitting of the lower of these doublets that is proportional to $1/n$. Because of the common-cation nature of the SL ordering potential, the upper doublet (of cation-s and anion-p character) will remain largely unsplit for all n. The SL X^{xy} valence-band edge will, however, behave quite differently from the (001) case for $n \geq 2$. In that case, it will be composed not of the X^{xy} VCA valence-band edge as in (001), but rather VCA states from the valley midway between X^x and X^y, which is the zinc-blende $\mathbf{k}$ point $2/3K_{\overline{1}10} = (\pi/a)(-1,1,0)$. These two degenerate light-mass valleys [see Fig. 18(b)] will give rise to well-center resonant states, just as in the conduction band.

Comparison of Figs. 18(c), 18(d), and 2(c) show that the (110) SL conduction-band states at $\overline{L}$ and $\overline{L}'$ will behave just as in the (001) case, showing the well-center resonant level behavior characteristic of two interacting degenerate light-mass valleys. The extreme light mass of the two $\overline{L}'$ valleys means that this resonant level behavior will persist for longer repeat periods n before the Kronig-Penney localization behavior eventually sets in. We expect similar resonant level behavior in the valence-band edge at $\overline{L}'$, but the dispersion of the VCA states forming the $\overline{L}$ valence-band edge is sufficiently flat [see Fig. 18(c)] that the SL states will probably fall down from their well centers and become somewhat localized, even in the ultrathin limit. Note that the purely flat dispersion seen in Fig. 2(c) is not seen here, however.

Consider now the case of (201) SL's [we consider here (20$\overline{1}$) for convenience]. A SL state at a given point $\mathbf{k}$ in the SL zone will be composed of VCA zinc-blende states along the line $\mathbf{k} \pm (2\pi/a)(2,0,-1) = \mathbf{k} \pm 2W_{x\overline{z}}$. As far as the main VCA Γ, X, and L points are concerned, the resulting folding relationships are just as in the (001) case: the Γ and X^z points are folded on top of each other, as are X^x and X^y, and L_{111} and $L_{11\overline{1}}$ [$\overline{L} = \overline{L}'$ by point-group symmetry now, unlike in the (110) case]. The full band foldings are shown in Fig. 19. It is seen that the SL valence-band edge at $\overline{\Gamma}$ will, as in every case, behave like a single-valley Kronig-Penney state. Note that the extreme lightness of the (201) Γ_{15v} masses will, however, substantially delay (with increasing n) the onset of GaAs localization of the $\overline{\Gamma}$ SL valence-band-edge states. A similar conclusion holds for the conduction-band-edge X^z states: the (201) X^z conduction-band mass is enormously lighter than its (001) or (110) counterparts, which will greatly delay the localization into the GaP X^z well. Note that the general n dependence of intervalley mixing (see Appendix A) implies a weak Γ-X^z coupling in ternary chalcopyrite systems, since these are $n=2$ (201) SL's. This has in fact been observed for several systems by Wei and Zunger.[45,65] The SL states evolving from the folding of the X^{xy} VCA valleys will behave just as in the (110) case: the conduction-band levels mimic the (001) levels, while for $n \geq 3$, the SL valence-band edge will result from
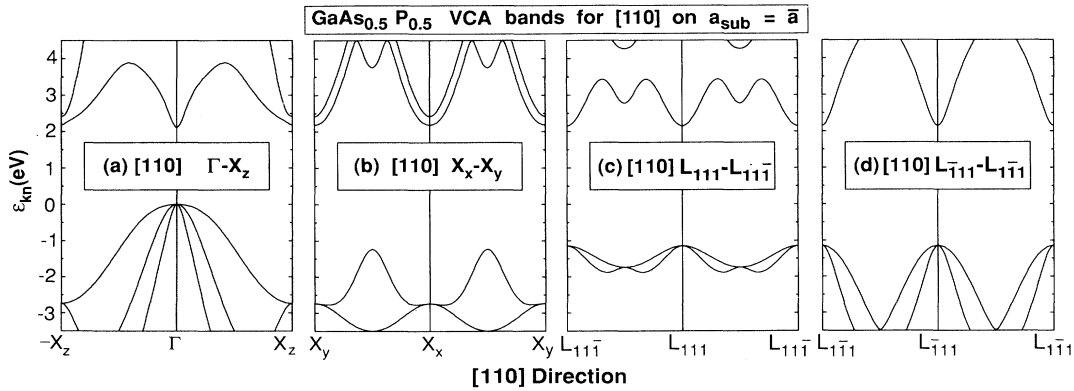
FIG. 18. Bands of the VCA Ga$\langle$AsP$\rangle$ zinc-blende compound along the (110) lines between the principal band-edge valleys.
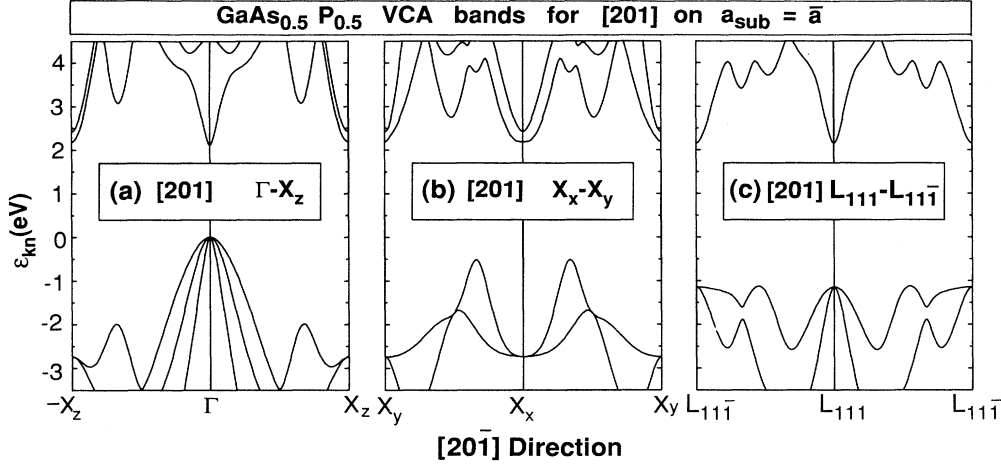
FIG. 19. Bands of the VCA Ga⟨AsP⟩ zinc-blende compound along the $(20\bar{1})$ lines between the principal band-edge valleys.

two degenerate intervening light-mass valleys 2 eV above the X^{xy} VCA valence-band-edge states. [These valleys occur at the zinc-blende **k** point $\frac{4}{9}K_{101}=(2\pi/3a)(1,0,1)$.] The SL conduction-band edge at $\bar{L}$ will again show the well-center resonant level behavior, while the $\bar{L}$ valence-band edge will behave as in (110), showing some Kronig-Penney localization even in the ultrathin limit of small n.

VII. CONCLUSION

Our major goal of this work has been to use the GaAs/GaP and GaAs/AlAs systems as paradigms for describing the physics of the evolution of SL levels in ultrathin systems. We begin by noting that using the VCA binary compound (at a lattice constant commensurate with that of the SL) as a parent compound from which the SL evolves gives rise to a SL ordering potential δV which is perturbatively small for these ultrathin systems. Since the VCA levels are approximately just the average of the constituents' band energies, this explains the common use of the average "alloy" levels as the parent energies from which the SL states evolve. Combining the fact that SL states at a point **k** in the SL zone are composed of VCA zinc-blende states along the line $\mathbf{k}\pm\frac{1}{2}\mathbf{G}$ (where **G** is a VCA binary reciprocal-lattice vector along the SL growth direction) with the fact that the smallness of δV means that only VCA states nearby in energy (within about 1 eV) are mixed, then allows one to predict the behavior of the resulting SL states. In particular, when n is sufficiently large or the VCA dispersion sufficiently flat that the SL band-edge state is composed of VCA states at neighboring $\delta\mathbf{k}=\mathbf{G}/2n$ from within the same valley, the resulting SL level has the typical Kronig-Penney behavior: its energy falls from its parent VCA's starting well-center position, and its wave function localizes a proportionate amount in one-half of the SL. Such behavior is generally found at the valence-band edge at $\bar{\Gamma}$ for all growth directions because of the involvement of only a single VCA valley. The amount of VCA dispersion away

from Γ_{15v}, which increases for the different growth directions in the order $(111)<(110)<(001)<(201)$, shows that the (111) $\bar{\Gamma}$ levels will localize into their quantum well most quickly (with increasing n), while the (201) $\bar{\Gamma}$ valence-band-edge levels will remain more resonant at the well center. Localized states similarly arising from *intra*valley mixing were also found for $n\geq 3$ in the SL conduction-band levels arising from the heavy mass (001) X^z_{1c} and (111) L_{1c} valleys.

In general, however, most SL states in these ultrathin $n\leq 3$ systems show a strong degree of *inter*valley mixing of VCA states. These arise both because of symmetry-forced intervalley degeneracies [e.g., due to the (001) folding relationships $\bar{M}=X^x+X^y$ and $\bar{L}=L_{111}+L_{11\bar{1}}$], and due to the fact that the conduction-band edges of a typical zinc-blende compound at Γ, X, and L are frequently within 1 eV of each other and thus can mix according to the folding relationships given in Eq. (2). Because the interface region is a significant portion of the total volume in these ultrathin SL's, such intervalley mixings can lead to large (up to 1 eV) level splittings and repulsions, and are thus a significant factor in determining the band structures of such systems. Furthermore, because such mixings generally occur *without* the involvement of VCA states from **k** points between the main two valleys (because the typical VCA dispersion is such that these states are too far away in energy for $n\leq 3$), the SL states evolve from a simple 2×2 Hamiltonian with off-diagonal element $U=\langle\psi_1(\mathbf{k})|\delta V|\psi_2(\mathbf{k}+\mathbf{G}/2)\rangle$. The resulting SL states will thus be resonant throughout the SL cell, and will evolve mainly from a well-center energy.

Analysis of the matrix element U leads to the following generic results regarding intervalley mixing in small n systems and the resulting well-center energy-level behavior. First, there is a generic n dependence to the coupling strength U, which is independent of the states involved. Its magnitude is very small for even n, and decays like $1/n$ for odd n from its maximal $n=1$ value. This holds true both for intervalley mixings away from the SL zone center between levels that are degenerate by symmetry,

and for the SL zone-center mixings between nondegenerate VCA states. The resulting level splittings and repulsions will thus have a similar n dependence. This explains the frequently seen strong downward bowing of $n=1$ SL levels from their average "alloy" level, and the generally much smaller bowing seen for $n=2$. It explains why the Γ-X^z coupling is small in ternary chalcopyrite systems, they being $n=2$ (201) SL's. For the case of zone-center mixings of nondegenerate VCA states, the amount of wave-function mixing (i.e., oscillator strength sharing) will also follow this n dependence (as long as the original VCA level splitting is not so small that one finds strong wave-function mixing even when U is small, as in the case of mixing degenerate VCA states). A second set of generic results we present is with regard to symmetry-imposed selection rules that govern the intervalley mixing. These control, for example, which of the two VCA conduction-band X minima mixes with Γ at the (001) SL zone center, and which of them splits at $\bar{M}$. (See Appendix B for these results.) A third generic result we obtained was regarding the differences between common-anion and common-cation ternary SL systems. For one, the above-mentioned selection rules are opposite for the two cases. This explains the occurrence of the $n=1$ (001) SL conduction-band edge at $\bar{L}$ in GaAs/AlAs (but at $\bar{M}$ in GaAs/GaP), since in this common-anion (common-cation) system only the upper (lower) X^{xy} conduction-band states split for odd n. Also, we noted much larger conduction-band intervalley coupling strengths U (and commensurately larger level splittings and repulsions) in the common-anion GaAs/AlAs system, as compared to the common-cation GaAs/GaP case, because of the cation character of the conduction-band states involved. The combination of all these principles of intervalley mixing allows for a semiquantitative description of SL levels in ultrathin systems.
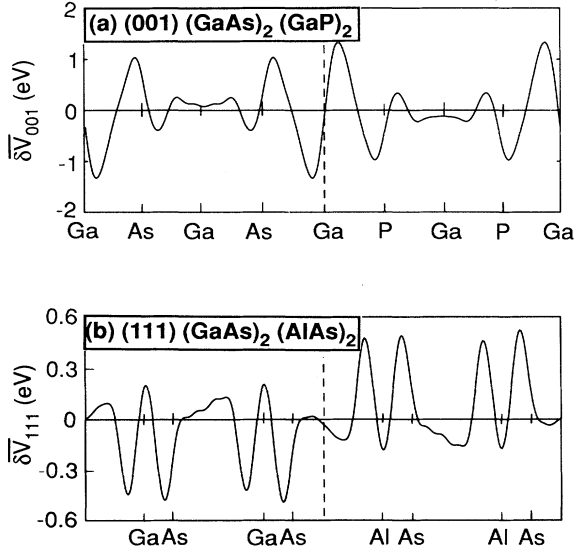
FIG. 20. Superlattice ordering potential δV for the (001) $(\text{GaAs})_2(\text{GaP})_2$ and (111) $(\text{GaAs})_2(\text{AlAs})_2$ SL's, averaged in planes orthogonal to the SL growth direction.

Finally, we also reported calculations on the (001) and (111) GaAs/GaP band offsets, appropriate to the coherent $a_\perp = \bar{a}$ interface. A large range of experimental values has been previously reported (varying by 0.4 eV), and our aim was to clarify these discrepancies. We found, for the strained constituents, that the difference in overall energy gaps was split in the valence-band–to–conduction-band ratio of 83:17 for (001) and 76:24 for (111). If a crude absolute deformation-potential model[60] is used to relate these strained binary energy levels to those of their unstrained parent compounds, these ratios become 67:33 for (001) and 77:23 for (111).

APPENDIX A: DEPENDENCE OF INTERVALLEY MIXING ON REPEAT PERIOD

In this appendix we analyze the n dependence of the matrix element $U = \langle \psi_1(\mathbf{k}) | \delta V | \psi_2(\mathbf{k}+\mathbf{G}/2) \rangle$ that controls the mixing of VCA states from valleys separated by half a reciprocal-lattice vector. Noting that the VCA states can be expressed as $\psi = e^{i\mathbf{k}\cdot\mathbf{r}} u(\mathbf{r})$ with $u(\mathbf{r})$ periodic in a VCA binary unit cell, this matrix element is

$$U = \int_{\text{SL cell}} d\mathbf{r}\, u_1^*(\mathbf{r}) u_2(\mathbf{r}) e^{i\mathbf{G}\cdot\mathbf{r}/2} \delta V(\mathbf{r}) \ . \tag{A1}$$

Defining the z' axis as parallel to the SL growth direction $\mathbf{G}$, this is

$$U = \int_{-L/2}^{L/2} dz'\, e^{iGz'/2} F(z') \ , \tag{A2}$$

where L is the SL period, and where

$$F(z') = \int dx'\, dy'\, u_1^*(\mathbf{r}) u_2(\mathbf{r}) \delta V(\mathbf{r}) \ . \tag{A3}$$

Limiting ourselves to the case of a ternary $(AC)_n(BC)_n$ SL with a common C atom, let us choose the $z'=0$ origin to lie at the interface midway between the two noncommon atoms. For a (001) SL, this will just be on a plane of common C atoms; for a (111) system, however, it will not lie on any atomic plane. Then the dependence of the matrix element U on the SL period n follows simply by noting that $F(z')$ is approximately odd in $z' \leftrightarrow -z'$ with respect to this origin. Since the $u_1^* u_2$ product in Eq. (A3) is periodic in VCA binary unit cells [there being n such cells both left and right of the origin in the z' integral of Eq. (A2)], the approximate oddness of $F(z')$ follows from the appropriate oddness of the $x'y'$ planar average of $\delta V(\mathbf{r})$, which we denote $\overline{\delta V}(z')$.

This function $\overline{\delta V}(z')$ is plotted in Fig. 20 for the (001) $(\text{GaAs})_2(\text{GaP})_2$ and (111) $(\text{GaAs})_2(\text{AlAs})_2$ SL's. It is obtained by subtracting the self-consistent VCA binary potential from the self-consistent SL potential, and then averaging the result in planes orthogonal to z'. As

shown, it is indeed approximately odd with respect to the interfacial origin. The approximate oddness of the function $\delta V(z')$ can be understood in terms of the decomposition of $\delta V(\mathbf{r})$ into a chemical and a strain component (see Sec. III A). Note that the *bare* perturbation $\delta V_{\mathrm{chem}}^{\mathrm{bare}}$ causing δV_{chem} is exactly odd in the $z' \leftrightarrow -z'$ VCA point-group operations.[66] This follows because the definition of the bare pseudopotential of the virtual $\langle AB \rangle$ ion, $V_{\langle AB \rangle} = (V_A + V_B)/2$, immediately implies $V_A - V_{\langle AB \rangle} = -(V_B - V_{\langle AB \rangle})$. Relating the self-consistent δV_{chem} to its bare counterpart by generalized linear and nonlinear VCA susceptibilities, so that

$$\delta V_{\mathrm{chem}} = \chi^{(1)} \delta V_{\mathrm{chem}}^{\mathrm{bare}} - \delta V_{\mathrm{chem}}^{\mathrm{bare}} \chi^{(2)} \delta V_{\mathrm{chem}}^{\mathrm{bare}} + \cdots , \qquad (A4)$$

we see that the screened δV_{chem} is also approximately odd in the $z' \leftrightarrow -z'$ operations of the VCA point group. (The only approximate nature of this oddness is due to the small nonlinear contribution to the screening.) The subsequent small elastic distortions along z' (in the case of lattice-mismatched constituents) give rise to a bare strain perturbation $\delta V_{\mathrm{str}}^{\mathrm{bare}}$ that is also approximately odd in $z' \leftrightarrow -z'$, because moving an ion at $z=0$ to its left changes the bare potential at $z<0$ opposite to the change at $z>0$, to first order in this change. The self-consistent δV_{str} is furthermore only approximately odd because even the pertinent linear susceptibility relating it to its bare counterpart is based on the unstrained SL, not on the VCA binary compound. In summary, apart from small nonlinearities in the screening process [i.e., $\chi^{(2)}$ in Eq. (A4)] and further nonlinearities due to the two-step nature of the chemical-plus-strain SL ordering process, the perturbations involved in creating $\delta V(\mathbf{r})$ are approximately odd in the $z' \leftrightarrow -z'$ point-group operations, and this results in an approximate oddness to $\delta V(z')$.

Having explained the origin of the oddness of $F(z')$ in Eq. (A3), we now note that this oddness immediately implies the $U(n)$ dependence noted in Sec. III. Since the two VCA states at $\mathbf{k}$ and $\mathbf{k}+\mathbf{G}/2$ are a zone face distance apart (i.e., *half* a reciprocal-lattice vector), their relative phase factor $e^{iGz'/2}$ oscillates with a period of *two* VCA binary unit cells, and the beating of this phase factor against the odd function $F(z')$ in Eq. (A2) leads to a $U(n)$ matrix element that nearly vanishes for even n and decays like $1/n$ for odd n. Note that this holds both for the case of mixing two VCA states that are degenerate by some space-group symmetry, and in the case of mixing two nondegenerate states (as occurs at the SL zone center), since no special requirements were made on the identities of $\psi_1(\mathbf{k})$ and $\psi_2(\mathbf{k}+\mathbf{G}/2)$ above. Note also that this same reasoning explains the near vanishing of the diagonal matrix elements $\langle \psi_1(\mathbf{k}) | \delta V | \psi_1(\mathbf{k}) \rangle$ of δV: without the phase factor $e^{iGz'/2}$ in Eq. (A2), the resulting integral approximately vanishes for all n, because of the approximate oddness of $F(z')$.

APPENDIX B: DERIVATION OF SELECTION RULES

This appendix is devoted to the derivation of the selection rules that control the intervalley mixing discussed in the main text. In particular, we determine which matrix

elements $\langle \psi_{\mathbf{k}'\alpha'} | \delta V | \psi_{\mathbf{k}\alpha} \rangle$ are mandated to vanish by space-group symmetries, where $|\psi_{\mathbf{k}\alpha}\rangle$ are the principal band-edge VCA states involved, and δV is the SL ordering potential.

1. (001) superlattice levels at $\overline{\Gamma}$

For the conduction-band states at $\overline{\Gamma}$, there are three main VCA states involved: Γ_{1c}, X_{1c}^z, and X_{3c}^z. The SL ordering potential δV has, of course, the full symmetry of the SL space group $D_{2d}^5 = P\overline{4}m2$. Furthermore, since this space group remains symmorphic if the coordinate origin is fixed on a central anion (midway between the Ga interface planes) for odd n and on a central cation for even n, δV also has the full symmetry of the *point* group $D_{2d} = \overline{4}2m$ with this choice of origin. In that case, the selection rules can simply be determined by understanding the symmetry properties of the Γ_{1c}, X_{1c}^z, and X_{3c}^z VCA states under the point-group operations of D_{2d}. Understanding the symmetry properties of the VCA X^z states under D_{2d} is particularly easy, since the point group of $\mathbf{k}$ there is simply D_{2d} itself. Table V shows the operations of the point group D_{2d}, along with the character table of its irreducible representations. Note that the VCA Γ_{1c} state is purely s-like, and is thus completely symmetric under D_{2d}. The lower (upper) conduction-band-edge state[51] at X^z, however, is anion-s plus cation-p_z (cation-s plus anion-p_z), and is thus even or odd, depending on the origin, in D_{2d} operations that change z into $-z$. Note from Table V that the X_1 (X_3) representation is even (odd) in the two classes $2C_2'$ and $2S_4$ of D_{2d} that change z into $-z$. Therefore, with an anion origin the lower X state is X_{1c} and the upper one is X_{3c}, while for a cation origin this labeling is reversed (the lower X state now being odd in $z \leftrightarrow -z$, being labeled X_{3c}). Since X_{3c}^z is odd in the $z \leftrightarrow -z$ operations of D_{2d}, while Γ_{1c}, X_{1c}^z, and δV are even in them, the selection rules governing the intervalley mixing at $\overline{\Gamma}$ are simply

$$\langle \Gamma_{1c} | \delta V | X_{3c}^z \rangle = 0 \qquad (B1)$$

TABLE V. The point group D_{2d}, together with its character table. The particular realization shown here is for the point group of $\mathbf{k}$ at X^z in the zinc-blende Brillouin zone, and at $\overline{\Gamma}$ and $\overline{M}$ in the (001) SL zone.

Class	Operations
E	E
C_2	$C_{2z} = \overline{x}\,\overline{y}z$
$2C_2'$	$C_{2x} = x\overline{y}\,\overline{z}$; $C_{2y} = \overline{x}y\overline{z}$
$2S_4$	$JC_{4z} = y\overline{x}\,\overline{z}$; $JC_{4\overline{z}} = \overline{y}x\overline{z}$
$2\sigma_d$	$JC_{2xy} = \overline{y}\,\overline{x}z$; $JC_{2x\overline{y}} = yxz$

	E	C_2	$2C_2'$	$2S_4$	$2\sigma_d$
1	1	1	1	1	1
2	1	1	1	-1	-1
3	1	1	-1	-1	1
4	1	1	-1	1	-1
5	2	-2	0	0	0

and

$$\langle X_{1c}^z | \delta V | X_{3c}^z \rangle = 0 . \tag{B2}$$

2. (001) superlattice levels at $\overline{M}$

In this section we derive the selection rules governing the band-edge states at the $\overline{M}$ point in the (001) SL zone. The conduction-band edge at $\overline{M}$ is determined from the 4×4 Hamiltonian matrix $\langle X_{1c/3c}^{x/y} | \delta V | X_{1c/3c}^{x/y} \rangle$, and it is our present purpose to determine which of these matrix elements are forced to vanish by symmetry. As noted above, if the coordinate origin is fixed on a central anion for odd n and on a central cation for even n, δV has the full symmetry of the *point* group D_{2d} shown in Table V. Furthermore, the VCA basis states X_{1c}^{xy} and X_{3c}^{xy} also have D_{2d} as their point group of $\mathbf{k}$, their particular realizations of this group being given in Table VI, and their transformation properties under these operations being given in Table V. The first selection rule we derive is that

$$\langle X_1 | \delta V | X_3 \rangle = 0 , \tag{B3}$$

this holding regardless of the x or y origin of either of the X_1 or X_3 states involved. Note that the operation C_{2z} is common to the $2C_2'$ class of all three realizations of D_{2d} given in Tables V and VI. Equation (B3) then follows simply by noting that δV and any X_1 state are even under C_{2z}, while any X_3 state is odd under it. The second selection rule we derive is that

$$\langle X_3^x | \delta V | X_3^y \rangle = 0 . \tag{B4}$$

This follows simply by noting that δV and X_3^x are even under C_{2x}, while X_3^y is odd under it. (Notice that C_{2x} belongs to *different* classes in the X^x and X^y realizations of D_{2d} given in Table VI.) These two selection rules result in the structure of the 4×4 Hamiltonian matrix shown in Table II. Equation (B3) forces the two 2×2 off-diagonal blocks to vanish, while Eq. (B4) forces the two off-diagonal elements of the X_3 subblock to vanish (this latter requirement leading to the $X_3 \leftrightarrow \overline{M}_5$ compatibility relation).

The valence-band maxima levels at $\overline{M}$ evolve from four degenerate states: the X_{5v}^x doublet and the X_{5v}^y doublet. These $\overline{M}$ states are thus determined by the 4×4 Hamiltonian $\langle X_{5v}^{x/y} | \delta V | X_{5v}^{x/y} \rangle$. Because of the two dimensionality of the X_5 representation, the selection rules here are much more easily derived if we allow for an *infinitesimal* tetragonal distortion of the VCA zinc-blende cell, in order to split the X_{5v} doublets. When this is done, the point group of $\mathbf{k}$ at X^x and X^y is $D_2(222)$. It is a four-element–four-class group made of the operations E, C_{2x}, C_{2y}, and C_{2z}. The X_{5v}^x doublet (of D_{2d}) is split into X_{2v}^x

TABLE VI. Realizations of the point group D_{2d} as the point group of $\mathbf{k}$ at X^x and X^y in the zinc-blende Brillouin zone.

Class	X^x operations	X^y operations
E	E	E
C_2	C_{2x}	C_{2y}
$2C_2'$	C_{2y}, C_{2z}	C_{2x}, C_{2z}
$2S_4$	$JC_{4x}, JC_{4\bar{x}}$	$JC_{4y}, JC_{4\bar{y}}$
$2\sigma_d$	$JC_{2yz}, JC_{2y\bar{z}}$	$JC_{2xz}, JC_{2x\bar{z}}$

and X_{3v}^x singlets (of D_2), while the X_{5v}^y doublet is split into X_{2v}^y and X_{4v}^y. This immediately implies a 4×4 Hamiltonian matrix with zeros positioned exactly as in Table II, since the two X_{2v} states form a 2×2 subblock, while the other two X_{3v} and X_{4v} states form two 1×1 subblocks (no interactions allowed between states of different D_2 representations because δV is totally symmetric under all four D_2 operations).

3. (001) superlattice levels at $\overline{L}$

Superlattice levels at $\overline{L}$ evolve from VCA zinc-blende states at L_{111} and $L_{11\bar{1}}$, plus, if $n \geq 2$, states from $\mathbf{k}$ points on the (001) adjoining line. The point group of $\mathbf{k}$ at L_{111} and $L_{11\bar{1}}$ is the six-element group C_{3v}. The only nonidentity element common to both the L_{111} and $L_{11\bar{1}}$ realizations of this group is, however, the reflection $JC_{2x\bar{y}}$. This operation is also a member of the (001) SL point group D_{2d} (see Table V), and the SL ordering potential δV thus has it full symmetry. The conduction-band edge at $\overline{L}$ evolves from the two degenerate $L_{111,1c}$ and $L_{11\bar{1},1c}$ zinc-blende states. These two states are allowed to mix by symmetry because they, like δV, are even under $JC_{2x\bar{y}}$. Symmetry-imposed selection rules do, however, block diagonalize the Hamiltonian pertinent to the valence-band-edge levels at $\overline{L}$. These levels are composed of two separate doublets $L_{111,3v}$ and $L_{11\bar{1},3v}$, plus states along the flat band connecting these two [see Fig. 2(c)]. The L_{3v} doublet is composed of both an even and odd state under $JC_{2x\bar{y}}$ (this being most easily seen by creating an *infinitesimal* tetragonal distortion of the zinc-blende cell to split this doublet), while the flat band connecting L_{111} to $L_{11\bar{1}}$ is purely odd under $JC_{2x\bar{y}}$. Thus the even states within the L_{3v} doublets cannot mix with any of the odd states along the flat band connecting them. For this reason these even states form the resonant states at the center of the potential well, as described in Sec. IV C 5.

[1] L. Esaki and R. Tsu, IBM J. Res. Develop. **14**, 61 (1970).
[2] G. C. Osbourn, J. Vac. Sci. Technol. B **1**, 379 (1983).
[3] *Molecular Beam Epitaxy and Heterostructures*, edited by L. L. Chang and K. Ploog (Nijhoff, Dordrecht, 1985).
[4] T. P. Pearsall, J. Bevk, L. C. Feldman, J. M. Bonar, J. P. Mannaerts, and A. Ourmazd, Phys. Rev. Lett. **58**, 729 (1987); J.

Vac. Sci. Technol. B **15**, 1274 (1987); J. Bevk, A. Ourmazd, L. C. Feldman, T. P. Pearsall, J. M. Bonar, B. A. Davison, and J. P. Mannaerts, Appl. Phys. Lett. **50**, 760 (1987).
[5] *Interfaces, Quantum Wells, and Superlattices*, edited by C. R. Leavens and R. Taylor (Plenum, New York, 1988).
[6] *Band Structure Engineering in Semiconductor Microstructures,*

edited by R. A. Abram and M. Jaros (Plenum, New York, 1989).

[7]J. Schulman and T. C. McGill, Phys. Rev. Lett. **39**, 1680 (1977).

[8]Y.-T. Lu and L. J. Sham, Phys. Rev. B **40**, 5567 (1989); L. J. Sham and Y.-T. Lu, J. Lumin. **44**, 207 (1989).

[9]M. A. Gell, D. Ninno, M. Jaros, D. J. Wolford, T. F. Keuch, and J. A. Bradley, Phys. Rev. B **35**, 1196 (1987).

[10]W. Ge, M. D. Sturge, W. D. Schmidt, L. N. Pfeiffer, and K. W. West, Appl. Phys. Lett. **57**, 55 (1990).

[11]S.-H. Wei and A. Zunger, J. Appl. Phys. **63**, 5794 (1988).

[12]S. Froyen, D. M. Wood, and A. Zunger, Phys. Rev. B **37**, 6893 (1988).

[13]A. Gomyo, T. Suzuki, and S. Iijima, Phys. Rev. Lett. **60**, 2645 (1988); S. R. Kurtz, J. M. Olson, J. P. Goral, A. Kibbler, and E. Beck, J. Electron. Mater. **19**, 825 (1990).

[14](a) H. R. Jen, M. J. Cherng, and G. B. Stringfellow, Appl. Phys. Lett. **48**, 1603 (1986); (b) T. S. Kuan, W. I. Wang, and E. L. Wilkie, *ibid.* **51**, 51 (1987); (c) A. Gomyo, T. Suzuki, A. Kobayashi, S. Katwata, I. Hino, and T. Yusasa, *ibid.* **50**, 673 (1987).

[15]M.-H. Meynadier, R. E. Nahory, J. M. Worlock, M. C. Tamargo, J. L. de Miguel, and M. D. Sturge, Phys. Rev. Lett. **60**, 1338 (1988).

[16]N. J. Pulsford, R. J. Nicholas, P. Dawson, K. J. Moore, G. Duggan, and C. T. B. Foxon, Phys. Rev. Lett. **63**, 2284 (1989).

[17]L. Brey and C. Tejedor, Phys. Rev. B **35**, 9112 (1987); Phys. Rev. Lett. **26**, 184 (19871).

[18]H. C. Liu, Appl. Phys. Lett. **51**, 1091 (1987).

[19]D. Z.-Y. Ting and Y.-C. Chang, Phys. Rev. B **36**, 4359 (1987).

[20]H. Akera, S. Wakakhara, and T. Ando, Surf. Sci. **196**, 694 (1988).

[21]L. D. L. Brown and M. Jaros, Phys. Rev. B **40**, 10 625 (1989).

[22]S. B. Zhang, M. S. Hybertson, M. L. Cohen, S. G. Louie, and D. Tomanek, Phys. Rev. Lett. **63**, 1495 (1989).

[23]J. S. Nelson, C. Y. Fong, and I. P. Batra, Appl. Phys. Lett. **50**, 1595 (1987).

[24]K. J. Moore, G. Duggan, and C. T. Foxon, Phys. Rev. B **38**, 5535 (1988).

[25]A. E. Blakeslee, J. Electrochem. Soc. **118**, 1459 (1971).

[26]P. L. Gourley, R. M. Biefeld, G. C. Osbourn, and I. J. Fritz, in *Proceedings of the 10th International Symposium on GaAs and Related Compounds, Albuquerque, 1982,* edited by G. E. Stillman (British Institute of Physics, Bristol, 1983), p. 249.

[27]P. L. Gourley and R. M. Biefeld, J. Vac. Sci. Technol. B **1**, 383 (1983).

[28]P. L. Gourley and R. M. Biefeld, Appl. Phys. Lett. **45**, 749 (1984).

[29]G. C. Osbourn, R. M. Biefeld, and P. L. Gourley, Appl. Phys. Lett. **41**, 172 (1982).

[30]G. C. Osbourn, J. Vac. Sci. Technol. **21**, 469 (1982); G. C. Osbourn, J. Appl. Phys. **53**, 1586 (1982).

[31]G. Armelles, J. M. Rodriquez, and F. Briones, Appl. Phys. Lett. **56**, 358 (1990).

[32]M. Recio, G. Armelles, J. Melendez, and F. Briones, J. Appl. Phys. **67**, 2044 (1990).

[33]P. Hohenberg and W. Kohn, Phys. Rev. **136**, B864 (1964).

[34]W. Kohn and L. J. Sham, Phys. Rev. A **140**, 1133 (1965).

[35]D. M. Ceperley and B. J. Alder, Phys. Rev. Lett. **45**, 566 (1980); J. P. Perdew and A. Zunger, Phys. Rev. B **23**, 5048 (1981).

[36]G. Kerker, J. Phys. C **13**, L189 (1980).

[37]J. Ihm, A. Zunger, and M. L. Cohen, J. Phys. C **12**, 4409 (1979).

[38]S. Froyen, Phys. Rev. B **39**, 3168 (1989).

[39]D. J. Chadi and M. L. Cohen, Phys. Rev. B **8**, 5747 (1973).

[40]G. A. Baraff, J. A. Appelbaum, and D. R. Hamann, Phys. Rev. Lett. **38**, 237 (1977); A. Baldereschi, S. Baroni, and R. Resta, *ibid.* **61**, 734 (1988).

[41]L. J. Sham and M. Schluter, Phys. Rev. Lett. **51**, 1888 (1983); J. P. Perdew and M. Levy, *ibid.* **51**, 1884 (1983).

[42]R. G. Dandrea and A. Zunger, Appl. Phys. Lett. **57**, 1031 (1990). In this publication we used a gap correction of 0.75 eV (rather than the 0.85 eV used here) because of an erroneous neglect of the spin-orbit splitting in comparison with the calculated energy gaps with experiment.

[43]An early study on $(GaAs)_n(AlAs)_m$ [J. Ihm, Appl. Phys. Lett. **50**, 1068 (1987)] calculated the X^{xy} levels to lie below X^z for $m \leq 7$, due to the neglect of second-neighbor tight-binding parameters, which results in an infinite transverse X mass.

[44]L. D. L. Brown, M. Jaros, and D. J. Wolford, Phys. Rev. B **40**, 6413 (1989).

[45]S.-H. Wei and A. Zunger, Appl. Phys. Lett. **56**, 662 (1989).

[46]H. M. Polatoglou, G. Kanellis, and G. Theodorou, Phys. Rev. B **39**, 8483 (1989).

[47]S. R. White and L. J. Sham, Phys. Rev. Lett. **47**, 879 (1981).

[48]J. Schulman and Y.-C. Chang, Phys. Rev. B **24**, 4445 (1981).

[49]The near equality of the VCA levels and the average of the levels of the constituents in the same zinc-blende structure with lattice constant $\bar{a}$ is well known. We are furthermore noting here that, due to the linearity of the deformation potentials involved, the VCA levels also remain the average of those of the appropriately strained constituents. Note that the resulting evolution of the SL levels from the *midpoint* of the wells formed by the constituent's band edges is due to the equal-period SL's considered here; consideration of a $(GaP)_1(GaAs)_3$ SL, for example, would show SL levels evolving from a position only 25% higher than the corresponding well.

[50]S. Froyen, D. M. Wood, and A. Zunger, Phys. Rev. B **36**, 4547 (1987).

[51]In this paper we refer to the lower (upper) X conduction-band edge as that with anion-s plus cation-p (anion-p plus cation-s) character, thus having X_1 (X_3) symmetry with an anion origin. This is correct for nearly all zinc-blende structures. Note, however, that GaSb, ZnTe, and HgTe have this order reversed, and the lower X state has X_3 symmetry with an anion origin.

[52]G. Ortiz, R. Resta, and A. Baldereschi (unpublished).

[53]R. W. G. Wycoff, *Crystal Structures,* 2nd ed. (Krieger, Malabar, Florida, 1982), Vol. 1, p. 110.

[54]R. G. Dandrea, J. E. Bernard, S.-H. Wei, and A. Zunger, Phys. Rev. Lett. **64**, 36 (1990).

[55]J. J. Hopfield, J. Phys. Chem. Solids **15**, 97 (1960).

[56]Su-Huai Wei (private communication).

[57]*Landolt-Börnstein New Series,* edited by O. Madelung, M. Schulz, and H. Weiss (Springer, Berlin, 1982), Vol. 17a. See pages 185–189 for the GaP band structure, and pages 218–224 for that of GaAs.

[58]M. E. Davis, G. Zeidenbergs, and R. L. Anderson, Phys. Status Solidi **34**, 385 (1969).

[59]A. D. Katnani and G. Margaritondo, Phys. Rev. B **28**, 1944 (1983). The earlier valence-band-offset value of 0.63 eV presented in this paper was later updated to 0.55 eV [see G. Margaritondo, Surf. Sci. **168**, 439 (1986)].

[60]D. L. Camphausen, G. A. N. Connell, and W. Paul, Phys. Rev. Lett. **26**, 184 (1981).

[61]C. G. Van de Walle and R. M. Martin, Phys. Rev. Lett. **62**,

2028 (1989); Phys. Rev. B **39**, 1871 (1989); R. Resta, L. Columbo, and S. Baroni, *ibid.* **41**, 12 358 (1990).

[62]J. Tersoff, in *Heterojunction Band Discontinuities: Physics and Device Applications,* edited by F. Capasso and G. Margaritondo (North-Holland, Amsterdam, 1987), p. 3.

[63]T. Nakayama and H. Kamimura, J. Phys. Soc. Jpn. **54**, 4726 (1985).

[64]These energies differ slightly from the results (1.97 and 2.83 eV) of a previous calculation [S.-H. Wei and A. Zunger, Appl. Phys. Lett. **53**, 2077 (1988)] due to the weighted average gap correction performed there.

[65]S.-H. Wei and A. Zunger, Phys. Rev. B **39**, 3279 (1989).

[66]S. Baroni, R. Resta, and A. Baldereschi, in *Band Structure Engineering in Semiconductor Microstructures,* edited by R. A. Abrams and M. Jaros (Plenum, New York, 1989), p. 51.